

 Open access • Posted Content • DOI:10.1101/2020.06.29.179234

## Centromere evolution in the fungal genus *Verticillium* — Source link

Michael F. Seidl, H. Martin Kramer, David Cook, Gabriel L. Fiorin ...+3 more authors

**Institutions:** Utrecht University, Wageningen University and Research Centre, Kansas State University, Sapienza University of Rome

**Published on:** 30 Jun 2020 - bioRxiv (Cold Spring Harbor Laboratory)

**Topics:** Heterochromatin, Centromere and Verticillium

Related papers:

- [Islands of retroelements are the major components of Drosophila centromeres](#)
- [Regional centromeres in the yeast \*Candida lusitanae\* lack pericentromeric heterochromatin](#)
- [Islands of retroelements are major components of Drosophila centromeres.](#)
- [Intergenic locations of rice centromeric chromatin.](#)
- [Long transposon-rich centromeres in an oomycete reveal divergence of centromere features in Stramenopila-Alveolata-Rhizaria lineages](#)

Share this paper:    

View more about this paper here: <https://typeset.io/papers/centromere-evolution-in-the-fungal-genus-verticillium-2wqllmh1ip>

1 **Centromere evolution in the fungal genus *Verticillium***

2 Michael F Seidl<sup>1,2#</sup>, H Martin Kramer<sup>2</sup>, David E Cook<sup>2,3</sup>, Gabriel Lorencini Fiorin<sup>2</sup>, Grardy CM  
3 van den Berg<sup>2</sup>, Luigi Faino<sup>2,4</sup>, and Bart PHJ Thomma<sup>2,5#</sup>

4

5 <sup>1</sup>Theoretical Biology & Bioinformatics, Utrecht University, Utrecht, the Netherlands

6 <sup>2</sup>Laboratory of Phytopathology, Wageningen University, Wageningen, the Netherlands

7 <sup>3</sup>Plant Pathology, Kansas State University, Manhattan, United States of America

8 <sup>4</sup>Environmental Biology Department, Sapienza Università di Roma, Rome, Italy

9 <sup>5</sup>University of Cologne, Institute for Plant Sciences, Cluster of Excellence on Plant Sciences  
10 (CEPLAS), 50674 Cologne, Germany

11

12 <sup>#</sup>Corresponding authors: [m.f.seidl@uu.nl](mailto:m.f.seidl@uu.nl) and [bart.thomma@wur.nl](mailto:bart.thomma@wur.nl)

13

14 Running title: Centromeres across the *Verticillium* genus

15 **ABSTRACT**

16 Centromeres are chromosomal regions that are crucial for chromosome segregation during  
17 mitosis and meiosis, and failed centromere formation can contribute to chromosomal anomalies.  
18 Despite this conserved function, centromeres differ significantly between and even within  
19 species. Thus far, systematic studies into the organization and evolution of fungal centromeres  
20 remain scarce. In this study, we identified the centromeres in each of the ten species of the fungal  
21 genus *Verticillium* and characterized their organization and evolution. Chromatin  
22 immunoprecipitation of the centromere-specific histone CenH3 (ChIP-seq) and chromatin  
23 conformation capture (Hi-C) followed by high-throughput sequencing identified eight conserved,  
24 large (~150 kb), AT-, and repeat-rich regional centromeres that are embedded in heterochromatin  
25 in the plant pathogen *V. dahliae*. Using Hi-C, we similarly identified repeat-rich centromeres in  
26 the other *Verticillium* species. Strikingly, a single repetitive element is strongly associated with  
27 centromeric regions in some but not all *Verticillium* species. Extensive chromosomal  
28 rearrangements occurred during *Verticillium* evolution, yet only a minority could be linked to  
29 centromeres, suggesting that centromeres played a minor role in chromosomal evolution.  
30 Nevertheless, the size and organization of centromeres differ considerably between species, and  
31 centromere size was found to correlate with the genome-wide repeat content. Overall, our study  
32 highlights the contribution of repetitive elements to the diversity and rapid evolution of  
33 centromeres within the fungal genus *Verticillium*.

34

35 **IMPORTANCE**

36 The genus *Verticillium* contains ten species of plant-associated fungi, some of which are  
37 notorious pathogens. *Verticillium* species evolved by frequent chromosomal rearrangements that  
38 contribute to genome plasticity. Centromeres are instrumental for separation of chromosomes  
39 during mitosis and meiosis, and failed centromere functionality can lead to chromosomal

40 anomalies. Here, we used a combination of experimental techniques to identify and characterize  
41 centromeres in each of the *Verticillium* species. Intriguingly, we could strongly associate a single  
42 repetitive element to the centromeres of some of the *Verticillium* species. The presence of this  
43 element in the centromeres coincides with increased centromere sizes and genome-wide repeat  
44 expansions. Collectively, our findings signify a role of repetitive elements in the function,  
45 organization and rapid evolution of centromeres in a set of closely related fungal species.

## 46 INTRODUCTION

47 Centromeres are crucial for reliable chromosome segregation during mitosis and meiosis. During  
48 this process, centromeres direct the assembly of the kinetochore, a multi-protein complex that  
49 facilitates attachment of spindle microtubules to chromatids (1-3). Failure in formation or  
50 maintenance of centromeres can lead to aneuploidy, i.e. changes in the number of chromosomes  
51 within a nucleus, and to chromosomal rearrangements (3-5). While these processes have been  
52 often associated with disease development (6), they can also provide genetic diversity that is  
53 beneficial for adaptation to novel or changing environments (7, 8). For example, aneuploidy in  
54 the budding yeast *Saccharomyces cerevisiae* can lead to increased fitness under selective  
55 conditions, such as the presence of antifungal drugs (9, 10). Thus, centromeric instability can  
56 contribute to adaptive genome evolution (11, 12).

57 Despite their conserved function, centromeres are among the most rapidly evolving  
58 genomic regions (13, 14) that are typically defined by their unusual (AT-rich) sequence  
59 composition, low gene and high repeat density, and heterochromatic nature (13, 15).  
60 Nevertheless, centromeres differ significantly in size, composition, and organization between  
61 species (13, 16). Centromeres in *S. cerevisiae* are only ~125 nucleotides long and are bound by a  
62 single nucleosome containing the centromere-specific histone 3 variant CenH3 (also called  
63 CENP-A or Cse4) (17-20). In contrast to these ‘point centromeres’, centromeres in many other  
64 fungi are more variable and larger, and have thus been referred to as ‘regional centromeres’ (15).  
65 For instance, in the opportunistically pathogenic yeast *Candida albicans*, the CenH3-bound 3-5  
66 kb long centromeric DNA regions differ significantly between chromosomes, and rapidly  
67 diverged from closely related *Candida* species (21-23). Centromeres in the basidiomycete yeasts  
68 *Malassezia* are similar in size (3-5 kb) but contain a short AT-rich consensus sequence in multiple  
69 *Malassezia* species (11). In *Malassezia*, chromosomal rearrangements and karyotype changes are  
70 driven by centromeric loss through chromosomal breakage or by inactivation through sequence

71 diversification (11). Chromosomal rearrangements at centromeres have been similarly observed  
72 in the yeast *Candida parapsilosis*, suggesting that centromeres can be fragile and contribute to  
73 karyotype evolution (11, 12). CenH3-bound centromeric regions of the basidiomycete yeast  
74 *Cryptococcus neoformans* are relatively large, ranging from 30 to 65 kb, and are rich in Long  
75 Terminal Repeat (LTR)-type retrotransposons (16). Centromere sizes differ between  
76 *Cryptococcus* species as those lacking RNAi and DNA methylation have shorter centromeres,  
77 associated with the loss of full-length LTR retrotransposons at centromeric regions, suggesting  
78 that functional RNAi together with DNA methylation is required for centromere stability (16).

79 In filamentous fungi, centromeres have been most extensively studied in the saprophyte  
80 *Neurospora crassa* (15). In this species, centromeric regions are considerably larger than in yeasts  
81 (on average ~200 kb), and are characterized by AT-rich sequences that are degenerated remnants  
82 of transposable elements and sequence repeats that lack an overall consensus sequence (15, 24,  
83 25). The increased AT-content and the degenerated nature of transposable elements in the  
84 genome of *N. crassa* are the result of a process called repeat-induced point mutation (RIP) (15,  
85 26). RIP has been linked to the sexual cycle of ascomycetes and targets repetitive sequences by  
86 inducing C to T mutations, preferably at CpA di-nucleotides (26). The AT-rich centromeric  
87 regions are bound by CenH3 and enriched in the heterochromatin-specific histone modification  
88 histone 3 trimethylation of lysine 9 (H3K9me3) (25). Additionally, H3K9me3 and cytosine  
89 methylation occurs at the periphery of the centromeres (25). Alterations in H3K9me3 localization  
90 compromise centromeric localization, suggesting that the formation and location of  
91 heterochromatin, rather than the DNA sequence itself, is essential for function and localization of  
92 centromeres in *N. crassa* (15, 25). However, heterochromatin is not a hallmark for centromeres in  
93 all filamentous fungi. Centromeres in the fungal wheat pathogen *Zymoseptoria tritici* are shorter  
94 (~10 kb) and AT-poor, and their presence does not correlate with transposable elements nor with  
95 heterochromatin-specific histone modifications such as H3K9me3 or histone 3 trimethylation of

96 lysine 27 (H3K27me3) (27). Thus, even though centromeric function is highly conserved, fungal  
97 centromeres differ considerably in size, sequence composition, and organization.

98 Knowledge on centromeres has been impaired by their repetitive nature, which hampers  
99 their assembly and subsequent analyses (15, 28). However, recent advances in long-read  
100 sequencing technologies enables to study the constitution and evolution of centromeres (11, 16,  
101 29-31). By using long-read sequencing technologies in combination with optical mapping, we  
102 previously generated gapless genome assemblies of two strains of the fungal plant pathogen  
103 *Verticillium dahliae* (32), whose genomes are characterized by genome rearrangements and the  
104 occurrence of lineage-specific (LS) regions (7, 8, 33-35) that are hypervariable between *V.*  
105 *dahliae* strains and contain genes with roles in adaptive evolution to plant hosts (7, 8, 33, 35).  
106 Repetitive elements within the LS regions display a distinct chromatin state when compared with  
107 other repetitive regions (36). The *Verticillium* genus consists of ten species that are all soil-borne  
108 and presumed asexual but have different life-styles (37). Nine of these species are haploid, while  
109 the species *Verticillium longisporum* is an allodiploid hybrid between a strain that is closely  
110 related to *V. dahliae* and an unknown *Verticillium* species (37-39). During the evolution of the  
111 different *Verticillium* species frequent chromosomal rearrangements occurred (8, 35, 40).  
112 Facilitated by the availability of high-quality genome assemblies of *V. dahliae* strains and of all  
113 other *Verticillium* species (32, 33, 40, 41), we here sought to identify and study the constitution  
114 and evolution of centromeres in the *Verticillium* genus.

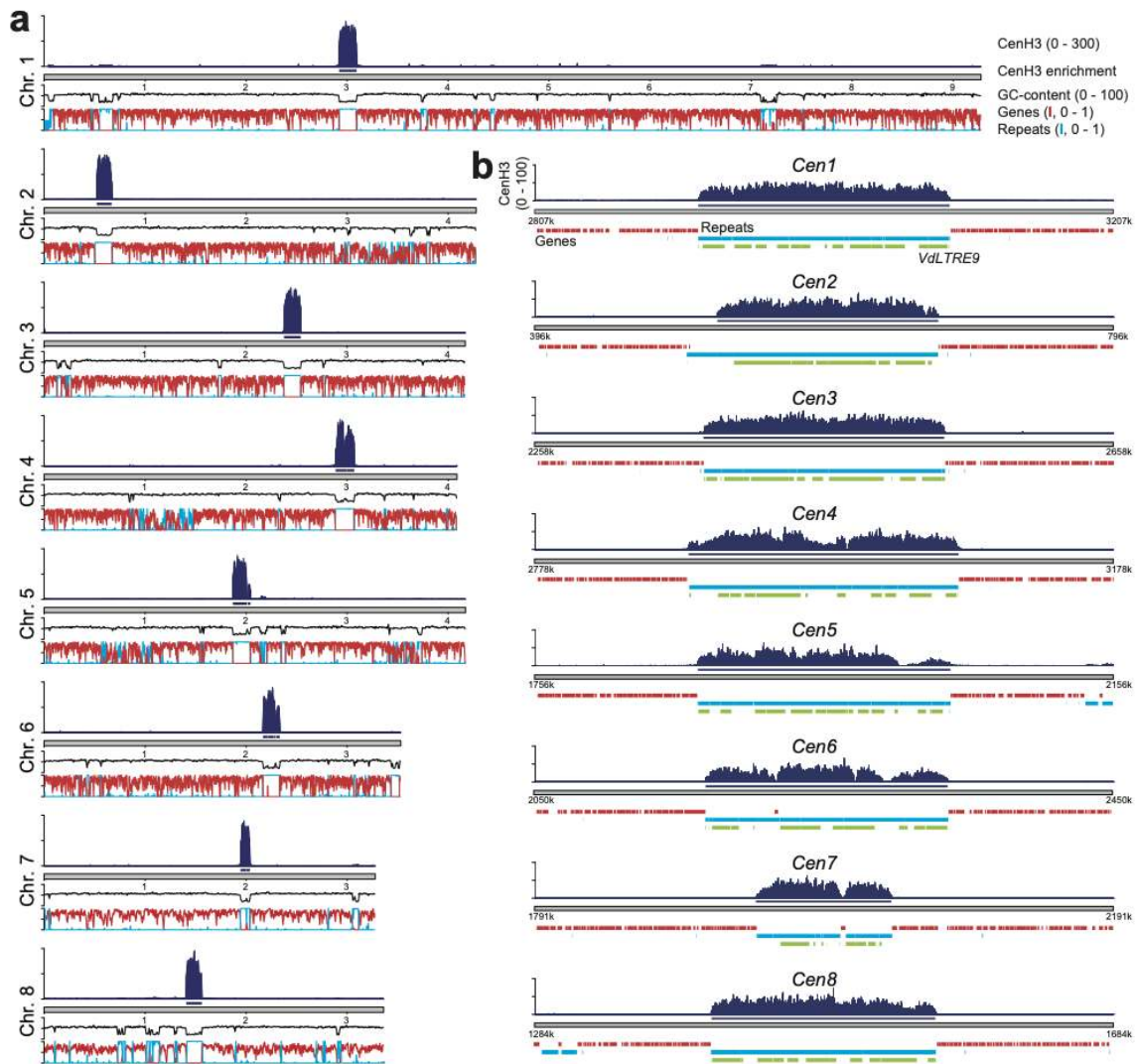
115 **RESULTS**

116 **CenH3-binding identifies large regional centromeres in *Verticillium dahliae***

117 Centromeres differ significantly between fungi, but most centromeres are functionally defined by  
118 nucleosomes containing CenH3 (1). To identify centromeres in *V. dahliae* strain JR2 by  
119 chromatin immunoprecipitation followed by high-throughput sequencing (ChIP-seq), we first  
120 identified the *V. dahliae* CenH3 ortholog (**Fig. S1a**) and generated transformants with N-  
121 terminally FLAG-tagged CenH3 (Table S1). To this end, the coding sequence for the FLAG-  
122 tagged CenH3 was inserted in locus behind the native *CenH3* promoter (**Figs. S1b-c**). We  
123 subsequently used anti-FLAG antibodies to purify FLAG-tagged CenH3-containing nucleosomes  
124 from two *V. dahliae* transformants (**Table S1a**) and sequenced the nucleosome-associated  
125 genomic DNA. Mapping of the sequencing reads to the *V. dahliae* strain JR2 genome assembly  
126 identified a single CenH3-enriched region per chromosome (**Fig. 1a; Fig. S1d-e**), while mapping  
127 of the sequencing reads derived from the WT strain did not reveal any CenH3-enriched region  
128 (**Fig. S1d-e**). The CenH3-enriched regions, designated as *Cen1-8*, range between ~94 and ~187  
129 kb in size (**Fig. 1a; Table 1**). To corroborate these centromere sizes, we assessed centromere  
130 locations based on a previously generated optical map (32, 35) revealing no significant size  
131 differences (**Fig. S1f**). Thus, we conclude that CenH3-binding defines large regional centromeres  
132 in *V. dahliae* strain JR2.

133





134  
135 **Figure 1 – CenH3-binding defines centromeres in *Verticillium dahliae* strain JR2.** (a)  
136 Schematic overview of the chromosomes of *V. dahliae* strain JR2 showing the normalized CenH3  
137 ChIP-seq read coverage (RPGC normalization in 1 kb bins with 3 kb smoothing), CenH3  
138 enriched regions, GC-content, gene density (red line), and repeat density (blue line). (b)  
139 Magnification of a 400 kb region containing the centromere is shown for each of the eight  
140 chromosomes of *V. dahliae* strain JR2 (*Cen1-8*) depicting the CenH3 ChIP-seq read coverage  
141 (RPGC normalization in 10 bp bins with a 30 bp smoothing) and enrichment, as well as the  
142 presence of genes (red) and repetitive elements (blue). Regions carrying the centromere-specific  
143 long-terminal repeat element *VdLTRE9* are highlighted in green.

144

145

146

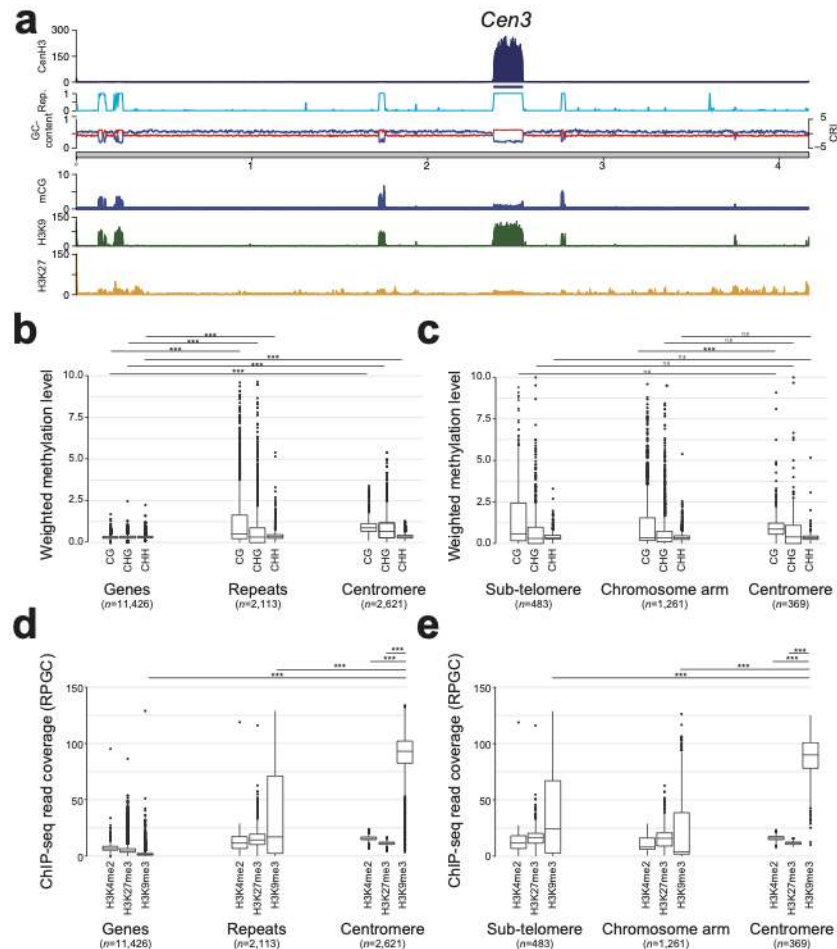
147 **Centromeres in *Verticillium dahliae* are repeat-rich and embedded in heterochromatin**

148 Centromeres are often characterized by increased AT-content, increased repeat density, and  
149 depletion of protein coding genes (13, 15, 29). To characterize the centromeres in *V. dahliae*  
150 strain JR2, we queried the eight chromosomes for the presence of large AT-rich, gene-sparse, and  
151 repeat-rich regions. Seven of the eight chromosomes contain only a single large (>93 kb; average  
152 size ~150 kb) AT-rich region (~74-78% versus ~46% genome-wide), nearly completely devoid of  
153 protein-coding genes and enriched for repetitive sequences, that overlaps with the regions defined  
154 by CenH3-binding (**Fig. 1a; Table 1**). In contrast, chromosome 1 contains three regions with  
155 these characteristics (**Fig. 1a; Table 1**). However, only one of these overlaps with the centromeric  
156 regions defined by CenH3-binding (**Fig. 1**).

157 Elevated AT-levels in repeat-rich regions are caused by RIP mutations in some  
158 filamentous fungi (15, 25, 26, 42). Due to its presumably asexual nature (7), the occurrence of  
159 RIP in *V. dahliae* is controversial (8, 43, 44), although signatures of RIP have previously been  
160 reported in a subset of repeat-rich regions (36). We assessed the occurrence of RIP signatures in  
161 centromeres using the composite RIP index (CRI) (45), which considers C to T mutations in the  
162 CpA context. Intriguingly, genomic regions located at centromeres display significantly higher  
163 CRI values than other genomic regions (e.g. genes or repetitive elements) (**Fig. 2a; Figs. S2,**  
164 **S3a**), and thus RIP signatures at repetitive elements located at centromeres likely contribute to the  
165 high AT-levels.

166 In most filamentous fungi and oomycetes, AT- and repeat-rich centromeres are embedded  
167 in heterochromatin that is characterized by methylated DNA and by particular histone  
168 modifications (H3K9me3 and H3K27me3) (13, 15, 16, 25, 30, 45). We recently determined  
169 chromatin states in the genome of *V. dahliae* strain JR2 and revealed that repetitive sequences  
170 outside of the LS regions display characteristics of heterochromatin (36). To define centromeric  
171 chromatin states, we used previously generated bisulfite sequencing data to monitor DNA

172 methylation (mC) and ChIP-seq data to determine the distribution of the heterochromatic marks  
173 H3K9me3 and H3K27me3 (36). To also determine the distribution of euchromatin, we performed  
174 ChIP-seq with an antibody against the euchromatic mark di-methylation of lysine 4 of histone H3  
175 (H3K4me2). We observed overall low genome-wide DNA methylation levels (36) (**Fig. 2a; Fig.**  
176 **S2**), similar to the previously reported levels for *Aspergillus flavus* (46) and lower than for *N.*  
177 *crassa* (47). Nevertheless, repetitive elements and centromeres show significantly higher DNA  
178 methylation levels in all contexts when compared with genes (**Fig. 2b**). Methylation (in CG  
179 context) at repetitive elements at centromeres is significantly higher than at repeats located along  
180 the chromosomal arm, but not at sub-telomeric regions (**Fig. 2c**), and more methylation at  
181 centromeres correlates with increased CRI (**Fig. 2a; Figs. S2, S3a**). DNA methylation co-  
182 localizes with H3K9me3 at repeat-rich regions (36) (**Figs. 2a; Fig. S2**). H3K9me3 occurs  
183 predominantly at repetitive elements localized at sub-telomeres and centromeres (**Figs. 2d-e;**  
184 **Figs. S2, S3b**). In comparison, H3K4me2 and H3K27me3 are largely absent from centromeres  
185 (**Figs. 2d-e; Fig. S3b**). Collectively, these observations indicate that centromeres of *V. dahliae*  
186 display typical characteristics of constitutive heterochromatin.



187

188 **Figure 2 – Centromeres in *Verticillium dahliae* strain JR2 are embedded in**

189 **heterochromatin.** (a) Schematic overview of chromosome 3 of *V. dahliae* strain JR2,

190 exemplifying the distribution of heterochromatin-associated chromatin modifications (mC,

191 H3K9me3, and H3K27me3) in relation to the centromeres. The different lanes display the

192 CenH3-FLAG ChIP-seq read coverage (RPGC normalization in 1 kb bins with 3 kb

193 smoothing), the CenH3-FLAG enriched regions, the repeat-density, the GC-content, the CRI as

194 well as the weighted cytosine methylation (all summarized in 5 kb windows with 500 bp slide),

195 and the normalized H3K9me3 and H3K27me3 ChIP-seq read coverage (RPGC normalization in 1

196 kb bins with 3 kb smoothing). The schematic overview of all chromosomes is shown in Figure

197 S2. (b) Box plots of weighted DNA methylation levels per genomic context (CG, CHG, or CHH)

198 are summarized over genes, repetitive elements, or 5 kb genomic windows (500 bp slide)

199 overlapping with the centromeric regions. (c) Weighted DNA methylation levels per genomic

200 context (CG, CHG, or CHH) are summarized over repetitive elements that have been split based

201 on their genomic location; sub-telomeres (within the first or last 10% of the chromosome),

202 centromeres, or the remainder of the chromosome arm. (d) ChIP-seq read coverage (RPGC

203 normalized; see (a)) for H3K4me2, H3K27m3, and H3K9me3 is summarized over genes,

204 repetitive elements, or 5 kb windows (500 bp slide) overlapping with the centromeric regions. (e)

205 ChIP-seq read coverage (RPGC normalized; see (a)) for H3K4me2, H3K27m3, and H3K9me3 is

206 summarized over repetitive elements that have been split based on their genomic location; sub-

207 telomeres (within the first or last 10% of the chromosome), centromeres, or the remainder of the

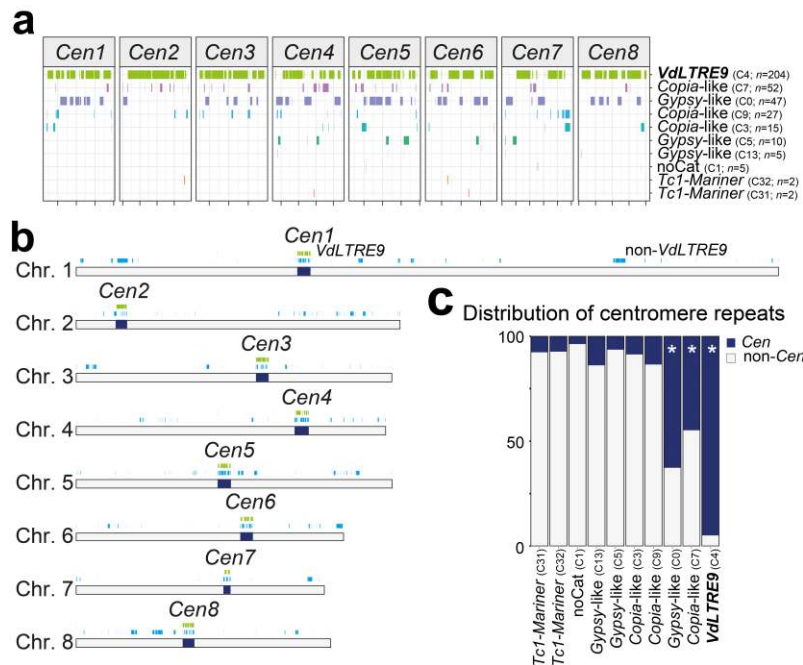
208 chromosomal arm. Statistical differences for the indicated comparisons were calculated using the  
209 one-sided non-parametric Mann-Whitney test; p-values < 0.001: \*\*\*.

210

### 211 **A single repeat associates with *Verticillium dahliae* strain JR2 centromeres**

212 Centromere identity and function is typically defined by CenH3-binding and not by specific DNA  
213 sequences, although various types of repetitive sequences, such as transposable elements, are  
214 commonly observed in centromeres of plants, animals, and fungi (13, 15, 48, 49). Unsurprisingly,  
215 CenH3-bound centromeres are repeat-rich in *V. dahliae* (**Fig. 1**). A detailed analysis of the eight  
216 centromeres revealed a near-complete (>96%) composition of repetitive elements belonging to  
217 only ten different repeat sub-families (**Figs. 1b, 3a; Table 1**), of which the majority shows  
218 similarity to LTR retrotransposons of the *Gypsy*- and *Copia*-like families (**Fig. 3a**). These  
219 elements show signs of RIP, are highly methylated, and non-transcribed (**Figs. S3c-e**), and thus  
220 likely inactive. Interestingly, a single LTR retrotransposon sub-family, previously designated  
221 *VdLTRE9* (8, 32), covers on average ~70% of the DNA sequences at the eight centromeres,  
222 ranging from 47% in *Cen7* to 83% in *Cen2* (**Fig. 3a; Table 1**). We scanned the genome for the  
223 localization of the ten repeat sub-families (**Fig. 3**). Intriguingly, although it is one of the most  
224 abundant repeats in the genome with 215 complete or partial matches, *VdLTR9* is associated to  
225 centromeres as 95% of the copies (204 out of 215; one-sided Fisher's exact test; multiple-testing  
226 corrected p-value 3e-106) occur at the eight centromeres, whereas only 5% of the copies are  
227 dispersed over the genome (**Fig. 3b-c**). The nine other repeat sub-families have additional  
228 matches that are located outside of the centromeres (**Figs. 1a; Figs. 3b-c**), and only two of these  
229 repeats are significantly enriched and consistently present in all eight centromeres; 63% and 45%  
230 of the matches of these two sub-families occur at the centromeres (**Fig. 3c**). Collectively, these  
231 findings suggest that only the presence of *VdLTRE9* is strongly associated with centromeres in *V.*  
232 *dahliae* strain JR2.

233 *VdLTRE9* displays similarity to LTR retrotransposons. The consensus sequence of  
 234 *VdLTRE9* is ~7.3 kb long (the two LTR sequences are each ~200 bp long), and the individual  
 235 matches share a high degree of sequence identity (~86%). Sequence similarity based TE-  
 236 classifications using PASTEC (50) indicates that the consensus sequence displays remote  
 237 similarity to *Gypsy*-like retrotransposons. Only ~25% of the *VdLTRE9* matches in the genome  
 238 cover the entire (>97.5%) consensus sequence, but many of these are still fragmented as they  
 239 occur as discontinuous copies. Furthermore, the *VdLTRE9* consensus sequence is AT-rich (~75%  
 240 AT), which may be caused by RIP (**Fig. S3d**), indicating that *VdLTRE9* has significantly  
 241 degenerated.



242 **Figure 3 – A single repeat family associates with centromeres in *Verticillium dahliae* strain**  
 243 **JR2.** (a) The presence of different repeat sub-families is shown across the eight centromeres  
 244 (*Cen1-8*), and the number of occurrences for each sub-family within the centromeres is indicated.  
 245 The individual centromeres in the diagram are shown in equal scale. (b) Genome-wide  
 246 distribution of the ten repeat sub-families occurring within the eight centromeres (*Cen1-8*;  
 247 dark blue); the location of *VdLTRE9* is shown in green and the location of elements belonging to the  
 248 other nine sub-repeat families (from panel (a)) is shown in light blue. (c) The distribution of  
 249 different repeat sub-families in centromeres (*Cen*; dark blue) and across the genome (non-*Cen*;  
 250 light grey). The enrichment of specific sub-families at centromeres was assessed using a one-  
 251 sided Fisher's exact test. Significant enrichment (multiple-testing corrected p-value < 0.01) is  
 252 denoted with an asterisk.  
 253

254

255 ***VdLTRE9* as hallmark of *Verticillium dahliae* centromeres**

256 To examine if *VdLTRE9* similarly occurs at centromeres in other *V. dahliae* strains, we made use  
257 of the complete genome assembly of *V. dahliae* strain VdLs17 (8, 32, 35). The evolution of *V.*  
258 *dahliae* is characterised by chromosomal rearrangements (8, 35) (**Figs. 4a; Figs. S4a-c**).  
259 Nevertheless, synteny analyses between *V. dahliae* strains JR2 and VdLs17 revealed large regions  
260 of co-linearity between chromosomes and identified significant sequence and synteny  
261 conservation between the centromeres and their flanking regions (**Figs. 4b-c; Fig. S4a**),  
262 suggesting that centromeric sequences and their locations are conserved. We queried the genome  
263 of *V. dahliae* strain VdLs17 for the presence of *VdLTRE9* and identified a single region on each  
264 chromosome, collectively containing 186 of the 207 (90%) complete or partial matches of  
265 *VdLTRE9* in the genome (**Fig. 4d**) (one-sided Fisher's exact test; multiple-testing corrected p-  
266 value 3e-146). These *VdLTR9*-rich regions are ~150 kb in size, AT-rich, gene-poor and repeat-  
267 rich, and share similarity to the previously identified CenH3-bound and *VdLTRE9*-enriched  
268 regions of *V. dahliae* strain JR2 (**Figs. 4b-c; Fig. S4d**), suggesting that these regions similarly  
269 represent the centromeres of *V. dahliae* strain VdLs17.

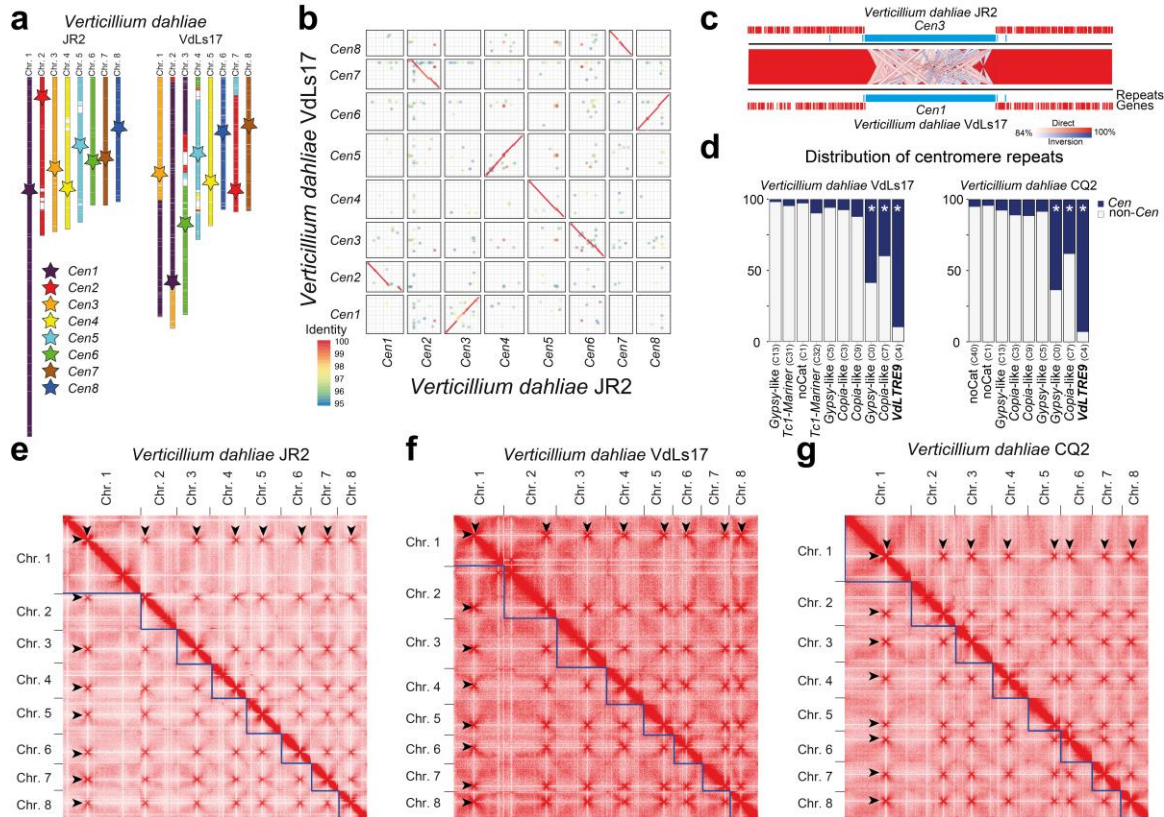
270 Centromeres *N. crassa* and some other fungi co-localize within the nucleus (15, 51-55). This  
271 co-localization can be experimentally determined using chromosome conformation capture (Hi-  
272 C), which can identify centromeres by their increased inter-chromosomal contacts (55). To  
273 confirm that Hi-C can be used to identify centromeres in *V. dahliae*, we first applied Hi-C to *V.*  
274 *dahliae* strain JR2. As anticipated, we observed seven strong inter-chromosomal contacts for each  
275 of the eight chromosomes (**Figs. 4e**). Importantly, the interacting regions overlap with the  
276 CenH3-bound regions that we identified as centromeres (**Table S1b**), demonstrating that  
277 centromeres in *V. dahliae* strain JR2 co-localize within the nucleus and supporting that Hi-C  
278 reliably identifies centromeres (51, 52). We then applied Hi-C to *V. dahliae* strain VdLs17, and

279 similarly identified regions with strong inter-chromosomal contacts, one for each of the  
280 chromosomes (**Figs. 4f**). These regions overlap with the *VdLTRE9*-enriched regions (**Table S1b**),  
281 suggesting that these represent functional centromeres in *V. dahliae* strain VdLs17.

282 The two *V. dahliae* strains JR2 and VdLs17 are closely related and differ only by ~0.05%  
283 sequence diversity (8, 35). Thus, the conservation of *VdLTRE9* at centromeres could be driven by  
284 limited divergence between the two *V. dahliae* strains rather than representing a hallmark of *V.*  
285 *dahliae* centromeres. Therefore, we sought to determine centromeres in an additional *V. dahliae*  
286 strain with increased sequence diversity when compared with *V. dahliae* strains JR2 or VdLs17,  
287 namely strain CQ2 that displays ~1.05 percent sequence diversity (33). We previously obtained a  
288 long-read based genome assembly of this strain that encompasses 17 contigs (33). We generated  
289 Hi-C data for *V. dahliae* strain CQ2 and utilized intra-chromosomal contacts to assign the contigs  
290 into eight pseudo-chromosomes, leaving ~148 kb unplaced scaffolds (**Fig. 4g; Fig. S4e; Table**  
291 **S1c**). We subsequently identified a single region with seven strong inter-chromosomal contacts  
292 for each pseudo-chromosome that is significantly enriched for *VdLTRE9* (one-sided Fisher's  
293 exact test; multiple-testing corrected p-value 3.4e-166) (**Figs. 4d, g; Fig. S4e; Table S1b**).  
294 Synteny analyses between *V. dahliae* strains JR2 and CQ2 revealed that the eight *VdLTRE9*-rich  
295 regions and their flanking chromosomal regions are co-linear, suggesting that centromere  
296 locations are conserved between different *V. dahliae* strains (**Figs. 4; Figs. S4a-c, f**). With an  
297 average size of 165 kb, the centromeres of *V. dahliae* strain CQ2 are similar in size as the 144 kb  
298 and 157 kb average sizes in *V. dahliae* strains VdLs17 and JR2, respectively (**Table S1b**). The  
299 sizes of the corresponding (i.e. homologous) centromeres vary between the different *V. dahliae*  
300 strains. Yet, the consistent co-occurrence of the *VdLTRE9*-rich regions with the interaction data  
301 obtained by Hi-C throughout a selection of *V. dahliae* strains demonstrates that *VdLTRE9* is a  
302 hallmark of *V. dahliae* centromeres.

303





304  
 305 **Figure 4 – Hi-C contact maps identify *VdLTRE9* as hallmark of centromeres in *Verticillium***  
 306 ***dahliae*.** (a) Synteny analyses of the eight chromosomes of *V. dahliae* strains JR2 and VdLs17.  
 307 Schematic overview of the eight chromosomes of *V. dahliae* strain JR2 (left) and the  
 308 corresponding syntenic regions in *V. dahliae* strains VdLs17 (right). Approximate locations of  
 309 centromeres are indicated by stars, and syntenic centromeres of *V. dahliae* strain VdLs17 are  
 310 colored according to *Cen1-8* of *V. dahliae* strain JR2. (b) Sequence alignment of the centromeric  
 311 regions  $\pm 20$  kb in *V. dahliae* strain JR2 and the corresponding regions in *V. dahliae* strains  
 312 VdLs17 shown as dot-plot. For clarity, only alignments with  $>95\%$  sequence identity are  
 313 displayed. (c) Magnification of *Cen3* of *V. dahliae* strain JR2 and the syntenic *Cen1* of strain  
 314 VdLs17. Synteny between regions is indicated by ribbons; entire centromeric regions *Cen1* and  
 315 *Cen3* are syntenic and sequence similarity between individual *VdLTRE9* elements is visualized.  
 316 The *Cen* regions  $\pm 150$  kb are shown as well as genes (red) and repeats (blue) are annotated  
 317 within this region. (d) Distribution of different repeat families in centromeres (*Cen*; dark blue)  
 318 and across the genome (non-*Cen*; light grey) for *V. dahliae* strains VdLs17 and CQ2. The  
 319 enrichment of specific sub-families at centromeres was assessed using a one-sided Fisher's exact  
 320 test. Significant enrichment (multiple-testing corrected  $p$ -value  $< 0.01$ ) is denoted with an  
 321 asterisk. (e-g) Hi-C contact matrix showing interaction frequencies between genomic regions in  
 322 *Verticillium dahliae* strains JR2 (e), VdLs17 (f), and CQ2 (g). Regions of high inter-chromosomal  
 323 interaction frequencies are indicative of centromeres and are highlighted by arrow heads.  
 324 Interaction frequencies are summarized in 50 kb bins along the genome.  
 325

326

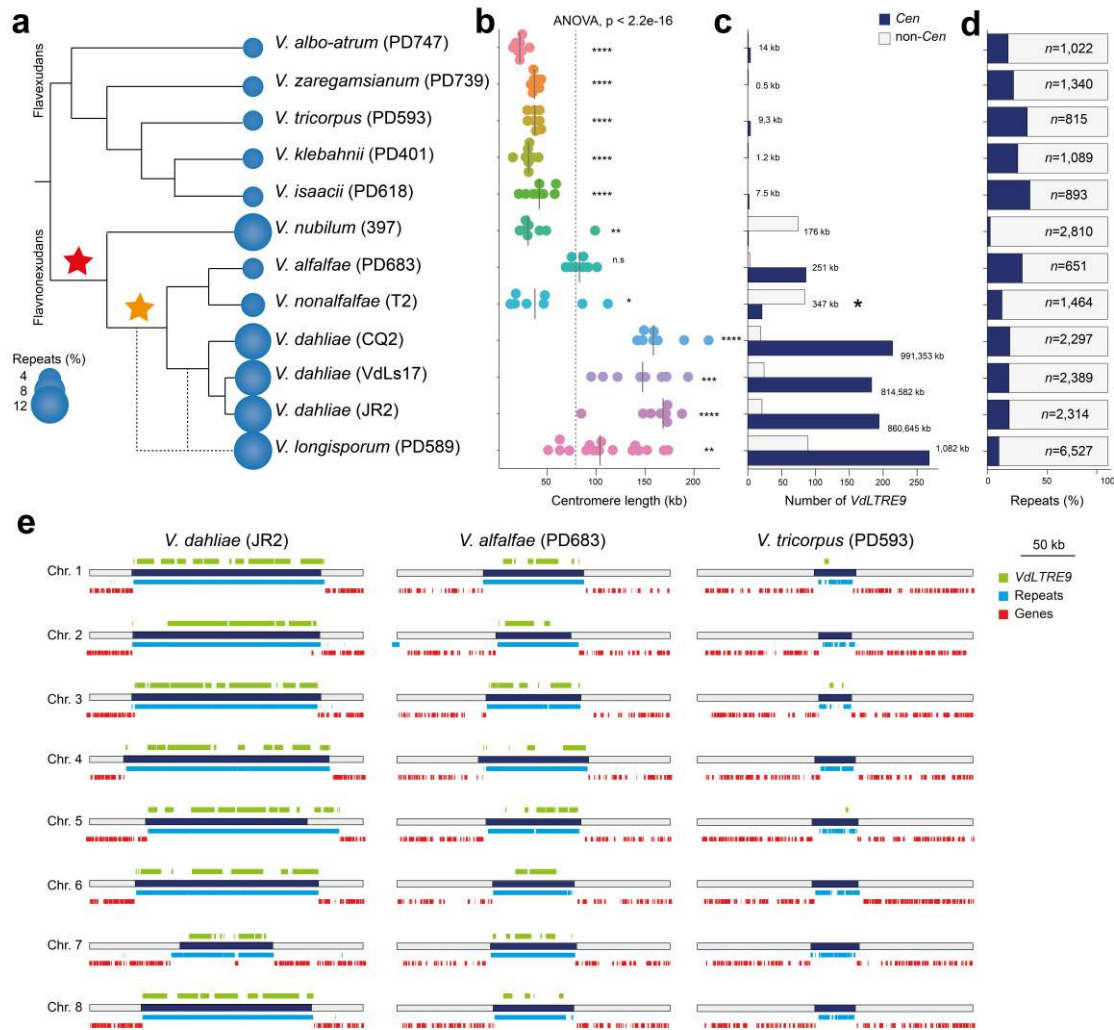
## 327 **The evolution of *Verticillium* centromeres**

328 In addition to *V. dahliae*, we previously generated genome assemblies of the eight haploid  
329 *Verticillium* species and the allodiploid *V. longisporum* (39, 40) (**Fig. 5a**) that ranged from 12 to  
330 684 scaffolds (**Table S1c**). These ten *Verticillium* species have been traditionally separated over  
331 two distinct clades; Flavnonexudans and Flavexudans (**Fig. 5a**) (37). We generated Hi-C data to  
332 study the composition and evolution of centromeres in the different *Verticillium* species. By using  
333 intra-chromosomal interaction signals, we first assigned the vast majority of the previously  
334 assembled contigs into eight pseudo-chromosomes for each of the haploid *Verticillium* species  
335 and 16 pseudo-chromosomes for the diploid *V. longisporum*, leaving between 0.5 kb and 2,022 kb  
336 unassigned (**Fig. S5; Table S1c**). For most genome assemblies, the pseudo-chromosomes contain  
337 one or both telomeric repeats (**Table S1c**), and thus we conclude that all *Verticillium* strains have  
338 eight chromosomes, and that this number doubled in *V. longisporum*. Based on the inter-  
339 chromosomal Hi-C interaction signals, we identified a single region with high inter-chromosomal  
340 contacts for each of the pseudo-chromosomes (**Fig. S5; Table S1d**), indicating that these are the  
341 centromeres in the different *Verticillium* species. The average centromere size in *Verticillium* is  
342 ~80 kb, yet we observed significant differences between the species (**Fig. 5b; Figs. S6a-b**).  
343 Centromeres within the Flavexudans clade are similarly sized and significantly smaller than the  
344 genus-wide average. By contrast, *V. dahliae* and *V. longisporum* centromeres are significantly  
345 larger.

346 We subsequently assessed whether *VdLTRE9* defines centromeres in the other  
347 *Verticillium* species besides *V. dahliae* as well. Interestingly, *VdLTRE9* is abundant at  
348 centromeres in the allodiploid *V. longisporum* and in *V. alfalfae*, but fewer (21) or no *VdLTRE9*  
349 copies were identified at centromeres in *V. nonalfalfae* and *V. nubilum*, respectively (**Fig. 5c; Fig.**  
350 **S6c-d**). Similarly, only few or no (partial) matches of *VdLTRE9* consensus could be identified in  
351 the genomes of the Flavexudans species (**Fig. 5c; Fig. S6-7; Table S1e**). Collectively, these

352 findings demonstrate that *VdLTRE9* is specific to Flavnonexudans species and has likely been  
353 recruited to the centromere only after the divergence of *V. nubilum* (**Fig. 5a; Fig. S6-7**).

354         Since *VdLTRE9* occurs only in few *Verticillium* species, we assessed to which extent  
355 other repetitive elements contribute to centromere organization. We analyzed the repeats  
356 identified by *de novo* repeat predictions for each of the *Verticillium* species. Centromeres in all  
357 species are AT- and repeat-rich (**Fig. S6a-b**), and some repeats occur in high frequency or nearly  
358 exclusively at centromeres in species that lack *VdLTRE9* (**Table S1e**). However, in contrast to  
359 *VdLTRE9*, these repeats cover only a minority (typically less than 10%) of the centromeres  
360 (**Table S1e**). Sequence similarity-based cluster analyses of the *de novo* repeat consensus  
361 sequences revealed that divergent repeat families contribute to *Verticillium* centromere  
362 organization (**Fig. S8**). Thus, in contrast to *VdLTRE9* in most Flavnonexudans species, we could  
363 not identify any additional repeat family as a hallmark of centromeres in other *Verticillium*  
364 species.



365  
 366 **Figure 5 – Evolution of centromeres in the genus *Verticillium*.** (a) Relationship of the ten  
 367 members of the genus *Verticillium*. The predicted repeat content for each of the genomes is  
 368 indicated (see Table S3 for details). The red star indicates the acquisition of *VdLTRE9* in the  
 369 Flavonoxudans clade while the yellow star indicates the recruitment of *VdLTRE9* into  
 370 centromeres. (b) Comparison of estimated centromere lengths (in kb) in the different *Verticillium*  
 371 spp. Each dot represents a single centromere and the line represents the median size. (c) The  
 372 number of (partial) *VdLTRE9* matches identified in centromeres (*Cen*; dark blue) and across the  
 373 genome (non-*Cen*; light grey). The asterisk indicates the high number of *VdLTRE9* elements in  
 374 unassigned contigs for *Verticillium nonalfalfae* strain T2 (see text for details). (d) Proportion of  
 375 predicted repeat content localized at centromeres (*Cen*; dark blue) and across the genome (non-  
 376 *Cen*; light grey). (e) Schematic overview of the eight centromeric regions (250 kb) in *Verticillium*  
 377 *dahliae* strain JR2, and *Verticillium alfalfae* strain PD683 and *Verticillium tricorpus* stain PD593  
 378 as representatives for clade Flavonoxudans and clade Flavexudans, respectively. The  
 379 centromeres are indicated by dark blue bars. The predicted genes (red) and repeats (light blue) are  
 380 shown below each centromere, and location of (partial) *VdLTRE9* matches (light green) are  
 381 shown above each centromere. Global statistical differences for the centromere sizes was  
 382 calculated using one-way ANOVA, and differences for each species compared to the overall

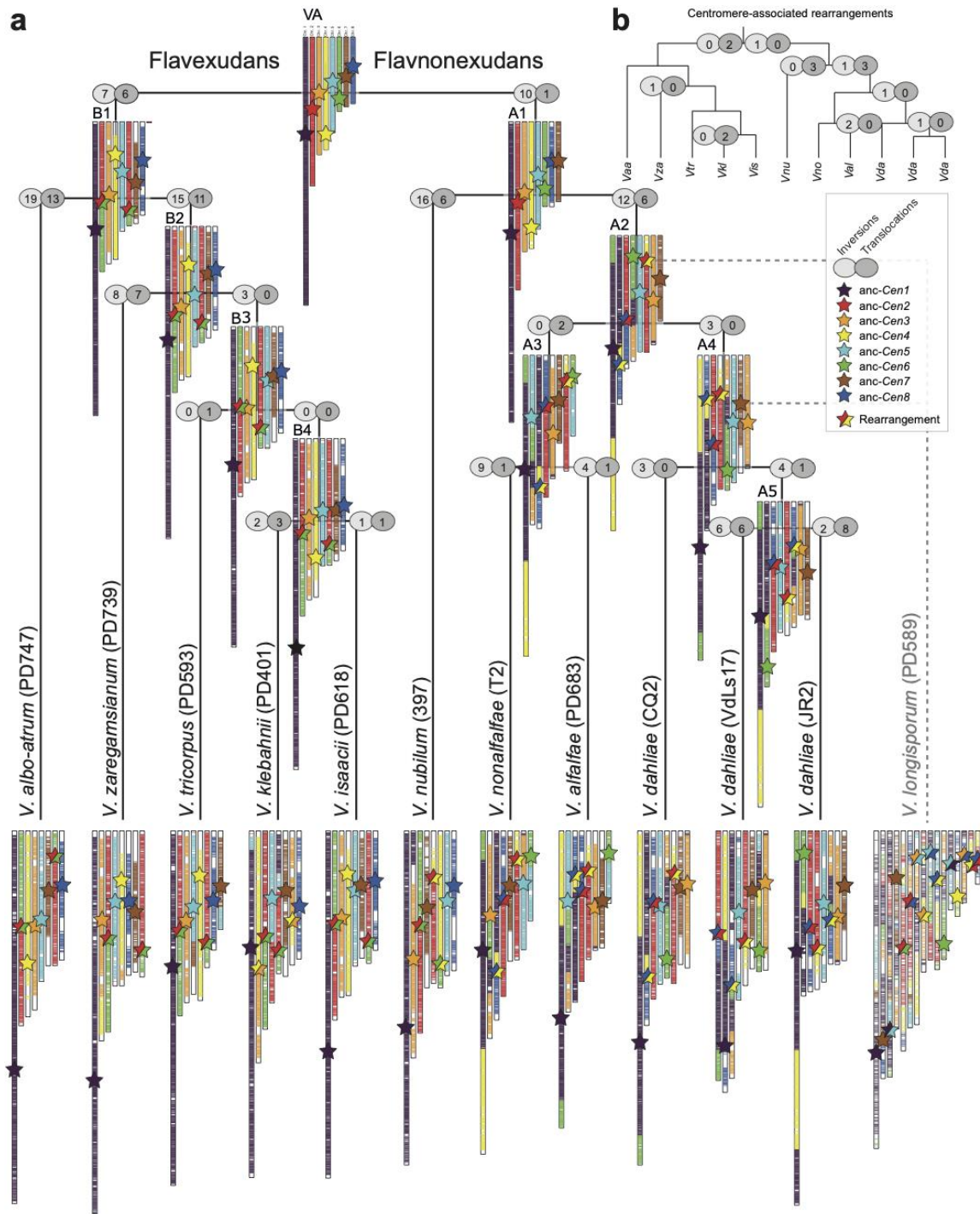
383 mean were computed using unpaired T-tests; p-values < 0.0001: \*\*\*\*, p-values < 0.001: \*\*\*, p-  
384 values < 0.01: \*\*, p-values < 0.05: \*.

385

### 386 **Centromeres contribute to *Verticillium* karyotype evolution**

387 We previously used fragmented genome assemblies to identify chromosomal rearrangements  
388 during *Verticillium* evolution (8, 35, 40). We hypothesize that centromeres might have  
389 contributed to these chromosomal rearrangements. To identify genome rearrangements and to  
390 trace centromeres during *Verticillium* evolution, we used the pseudo-chromosomes of the haploid  
391 *Verticillium* species to reconstruct ancestral chromosomal configurations using AnChro (**Fig 6a**)  
392 (56). We reconstructed all potential ancestors that predominantly had eight chromosomes and  
393 ~8,000 genes (**Figs. S9a-b**), yet the number of ancestral chromosomes and genes varied when  
394 approaching the last common ancestor (**Figs. S9a-b**). By balancing the number of reconstructed  
395 chromosomes and genes, we identified a single most parsimonious ancestral genome with eight  
396 chromosomes and ~8,500 genes (**Fig. 6a; Fig. S9c**), except for the last common ancestor within  
397 the clade Flavexudans clade that had eight major chromosomes and two additional  
398 ‘chromosomes’ with only six and two genes (**Fig. S9d**). As these two smaller ‘chromosomes’  
399 likely do not represent genuine chromosomes, we conclude that all of the ancestral genomes,  
400 similar to the extant haploid *Verticillium* genomes, had eight chromosomes (**Fig. 6a**). Confirming  
401 our previous report (40), we observed in total 198 chromosomal rearrangements (124 inversions  
402 and 74 translocations) (**Fig. 6a**). The number of chromosomal rearrangements is lower than  
403 previously recorded and we did not observe any chromosomal fusion or fission events, which is  
404 likely the result of the drastically improved genome assemblies, but the rearrangement signal on  
405 each branch is sufficient to nevertheless recapitulate the known *Verticillium* species phylogeny  
406 (**Fig. S9e**). Importantly, we observed 17 genomic rearrangements that occurred at, or in close  
407 proximity (within ~15 genes up or downstream) to, centromeres, both in extant *Verticillium*  
408 species as well as in the ancestors (**Fig. 6**). For example, at the branch from the last common  
409 ancestor (VA; **Fig. 6a**) to the ancestor of the clade Flavexudans (B1; **Fig. 6a**), two centromere-

410 associated translocations (between the ancestral chromosome 2 and 6) led to the formation of two  
411 rearranged chromosomes. In total, we observed that five out of the eight ancestral centromeres  
412 were associated with a chromosomal rearrangement at one point during evolution (**Fig. 6a**).  
413 Nevertheless, comparisons of protein-coding genes that flank centromeres show that these are  
414 syntenic in most extant species. Similarly, none of the recent chromosomal rearrangements  
415 observed between *V. dahliae* strains is associated with centromeres (**Figs. 4a-b, 6a**). Thus, while  
416 chromosomal rearrangements involving centromeres occurred during evolution, they do not  
417 account for the majority of the karyotype variation between extant *Verticillium* species.



418

419 **Figure 6 – Centromeres contribute to karyotype evolution in *Verticillium*.** (a) Relationship of  
 420 the ten members of the genus *Verticillium*. The allodiploidization event forming *V. longisporum*  
 421 is indicated by dashed lines (38, 57). The chromosomal evolution within the haploid members of  
 422 the genus was reconstructed using AnChro (56). The chromosomal structure of the nine species is  
 423 shown in relation to the last common ancestor of the genus. The approximate locations of the  
 424 centromeres are indicated by stars. The number of chromosomal rearrangements (inversions and  
 425 translocations) are displayed for each branch, and centromeres that co-localize in proximity to  
 426 chromosomal rearrangements are highlighted by two-colored stars. (b) The number of major

427 chromosomal rearrangements that occurred at, or in close proximity of, centromeres are shown  
428 along the branches depicting the *Verticillium* species phylogeny shown in (a).

429

## 430 **DISCUSSION**

431 Centromeric regions are among the most rapidly evolving genomic regions (13-16, 29), yet  
432 centromere evolution has only been systematically studied in few fungi (11, 12, 16, 29). Here, we  
433 took advantage of the fungal genus *Verticillium* and used a combination of genetic and genomic  
434 strategies to identify and characterize centromere organization and evolution. *Verticillium*  
435 centromeres are characterized as large regional centromeres that are repeat-rich and embedded in  
436 heterochromatin. We furthermore show that centromeres contribute to the karyotype evolution of  
437 *Verticillium*. Finally, we demonstrate that *VdLTRE9* is a hallmark of centromeres in some  
438 *Verticillium* species, while species that lack *VdLTRE9* display a divergent repeat content.

439         Centromeres in fungi, plants, and animals co-localize within the nucleus (15, 51-55, 58),  
440 a phenomenon that can be exploited for their identification (51, 52). Here, we used Hi-C to first  
441 establish chromosome-level genome assemblies and subsequently identify centromeres in every  
442 *Verticillium* species, and we demonstrate that centromere locations are in agreement with CenH3-  
443 binding. While we obtained chromosome-level genome assemblies for all species, Hi-C  
444 scaffolded genome assemblies could still contain partially collapsed repeats and assembly gaps, in  
445 particular for short-read assemblies (59). With the exception of *V. nonalfalfae*, we observed only  
446 few sequencing gaps and no evidence that would point to collapsed repeats at centromeres,  
447 suggesting that the inferred centromeres are of high quality. *Verticillium* centromere sizes differ ,  
448 which is likely not driven by assembly artefacts, and centromeres in most *Verticillium* species are  
449 larger than in *Z. tritici* (27), *C. neoformans*, *M. oryzae*, or *Fusarium graminearum* (13, 16, 29),  
450 yet smaller than in *N. crassa* (25). Species of the Flavexudans clade typically encode fewer  
451 repeats than species of the clade Flavnonexudans clade (32, 40, 60), and *V. nubilum*, *V.*  
452 *longisporum*, and *V. dahliae* are particularly rich in repeats when compared with other



453 *Verticillium* species (32, 39-41, 60). Thus, increased centromere sizes positively correlate with  
454 overall increased repeat contents.

455 Using fragmented genome assemblies, we previously identified chromosomal  
456 rearrangements during *Verticillium* evolution (8, 35, 40) that were thought to have contributed to  
457 genetic diversity and adaptation in the absence of sexual recombination (7, 35, 40). Chromosome-  
458 level genome assemblies for an entire genus enabled unprecedented analyses of the karyotype  
459 evolution over longer evolutionary timescales. Here, we observed extensive chromosomal  
460 rearrangements and provide evidence that some rearrangements at centromeres contributed to  
461 karyotype evolution, most of which occurred early during the divergence of *Verticillium*.  
462 Chromosomal rearrangements at centromeres occur in the fungal yeasts *Candida*, *Cryptococcus*,  
463 and *Malassezia* (11, 12, 61), and synteny breakpoints have been identified between mammals and  
464 chicken (62), suggesting that centromeres often contribute to karyotype evolution. The emergence  
465 of chromosomal rearrangements at centromeres could be facilitated by their repeat-rich nature  
466 (11, 12). For example, centromeres in *Malassezia* are enriched with an AT-rich motif that could  
467 facilitate replication fork stalling, which leads to double strand DNA breaks (11). Repeats  
468 localized outside of centromeres in *V. dahliae* contribute to chromosomal rearrangements (8), and  
469 thus it seems plausible that centromeric repeats similarly contribute to chromosomal  
470 rearrangements. Chromosomal rearrangements often do not only lead to changes in chromosome  
471 organization but also in chromosome number (11, 12). While we observed chromosomal  
472 rearrangements, all extant and ancestral genomes contained eight chromosomes, suggesting that  
473 eight chromosomes are a stable configuration for all *Verticillium* species.

474 Centromere position and function are thought to be driven by the protein complement  
475 (e.g. CenH3 localization) and by heterochromatin formation rather than by specific DNA  
476 sequences (13, 15, 63). In *V. dahliae*, we observed the co-occurrence of CenH3 with H3K9me3  
477 and DNA methylation. This suggests that DNA methylation, as previously reported in *N. crassa*

478 and in *C. neoformans* (16, 25), is also a feature of centromeric DNA in *V. dahliae*. Co-  
479 localization of CenH3 with H3K9me2/3 and DNA methylation has been reported for *N. crassa*  
480 (25) and *C. neoformans* (16). In contrast, H3K9me3 and H3K27me3 are absent from centromeres  
481 in *Z. tritici* (27). H3K4me2 borders most centromeres in *Z. tritici* (27), and is associated with  
482 centromeres in *S. pombe* and some animals and plants (64-67). H3K4me2 has not been observed  
483 at centromeres in most fungi, including *V. dahliae*, and in the oomycete *P. sojae* (30). Changes in  
484 heterochromatin in *N. crassa* leads to altered CenH3 positioning (25), suggesting that  
485 heterochromatin is similarly required for centromere maintenance and function in *V. dahliae*.  
486 Elevated AT-levels in repeat-rich heterochromatic regions can be caused by RIP mutations (15,  
487 25, 26, 42). RIP-like mutations have been previously reported in some repeats in *V. dahliae* (36,  
488 44), and we observed strong RIP signals at centromeres. Due to its presumably asexual nature (7),  
489 the occurrence of RIP in *V. dahliae* is controversial (8, 43, 44). Noteworthy, mutational signatures  
490 resembling RIP have recently been observed in *Z. tritici* propagated through mitotic cell  
491 divisions, pointing to the existence of a mitotic version of a RIP-like process (42). Thus, we  
492 conclude that RIP was an active process in *V. dahliae* at some point in evolution, or that RIP-like  
493 processes outside of the sexual cycle occur in *V. dahliae*.

494 Centromeres are often enriched for a variety of different retrotransposons and other  
495 repetitive elements (15, 16, 25, 29, 30). We similarly observed that centromeres in all *Verticillium*  
496 species are repeat-rich. Repeats and their remnants identified at centromeres typically also occur  
497 outside of centromeres, as observed in *M. oryzae* (29) and *N. crassa* (25). Strikingly, we observed  
498 that a single repetitive element, *VdLTRE9*, is strongly associated with centromeres in some  
499 *Verticillium* species, which to our knowledge, has only been observed in the fungus *Cryptococcus*  
500 where centromeres contain six retrotransposons (*Tcn1-6*) that nearly exclusively occur at  
501 centromeres (16). Similarly, centromeres of the oomycete plant pathogen *Phytophthora sojae*  
502 contain multiple types of repeats, but they are enriched for a single element called CoLT (*Copia-*

503 Like Transposon) (30). The strong associations of specific repeats to centromeres could directly  
504 or indirectly link these elements to centromere function. Functional centromeres as observed here  
505 are also heterochromatic and contain CenH3. AT-rich repetitive elements can direct  
506 heterochromatin formation via DNA methylation and H3K9me3 deposition in *N. crassa* (45, 68),  
507 a phenomenon that can also occur at repeats outside of centromeres (45). Heterochromatin  
508 occurs at centromeres but also at repeat-rich regions outside of centromeres in *V. dahliae*, thus the  
509 repeat-rich nature of centromeres is likely not sufficient to direct CenH3 deposition. In *S. pombe*  
510 heterochromatin formation is directed by short interfering RNAs (siRNA) derived from flanking  
511 repetitive elements via RNAi (69, 70), and RNAi and heterochromatin mediate CenH3  
512 localization at centromeres (71, 72). RNAi is also important for centromere maintenance and  
513 evolution in *Cryptococcus*, as RNAi deficient species have smaller centromeres than RNAi  
514 proficient ones (16). Interestingly, centromere-specific elements (*Tcn1-6*) in RNAi proficient  
515 species are typically full-length elements while only remnants can be found in RNAi deficient  
516 species, which could be caused by recombination between elements (16). In *Verticillium*,  
517 centromere size differences correlate with increase of repeat content and the recruitment of  
518 *VdLTRE9*, which is highly fragmented and likely non-active. Furthermore, even though key  
519 components of the RNAi machinery exist in at least some *Verticillium* species (73), we know  
520 very little about its biological functions. Similarly, to *C. neoformans*, we observed no  
521 transcriptional activity of *VdLTRE9* or any other repeat at centromeres, but it is unclear if this  
522 silencing is mediated by RNAi, is a consequence of their heterochromatic nature, is due to their  
523 fragmentation, or a combination of these. Ultimately, unravelling how specific elements  
524 contribute to centromere identity necessitates future experiments. *VdLTRE9* occurs only in some  
525 *Verticillium* species and has likely been recruited to centromeres subsequent to the divergence of  
526 *V. nubilum*. Conversely, these observations raise further questions on the roles of repeats and  
527 mechanisms of centromeric identity in species without *VdLTRE9*. Repeats are important drivers  
528 of *Verticillium* genome evolution and function (8, 36), and here we highlight their contributions

529 to centromere diversity within the fungal genus *Verticillium*. Our analyses provide the framework  
530 for future research into the diversity or convergence of mechanisms establishing centromere  
531 identity and functioning in fungi.

## 532 MATERIAL & METHODS

### 533 Construction of *Verticillium dahliae* transformants expressing FLAG-tagged CenH3

534 CenH3 and H3 homologs were identified in the predicted proteomes of *V. dahliae* strain JR2 (32)  
535 and selected other fungi through a BLAST sequence similarity search (blastp v2.9.0+; default  
536 settings, e-value cutoff 1e-20) (74, 75) using the *N. crassa* CenH3 (Q7RXR3) and H3 (P07041)  
537 sequences as queries. Missing homologs of CenH3 or H3 were identified using manual BLAST  
538 (tblastn v2.9.0+; default settings) (74, 75) and exonerate (v2.2.0; default settings) (76) searches  
539 against the genome sequences. Protein sequences of selected CenH3 and H3 proteins were  
540 aligned using mafft (v7.271; default settings, LINSi) (77). A phylogenetic tree was inferred with  
541 maximum-likelihood methods implemented in IQ-tree (v1.6.11) (78) and robustness was assessed  
542 by 1,000 rapid bootstrap replicates.

543 To construct the N-terminally FLAG-tagged CenH3 strain of *V. dahliae*, a recombinant  
544 DNA fragment was constructed into the binary vector PRF-HU2 (79) or PRF-GU2 for  
545 homologous recombination. The CenH3 locus, from *V. dahliae* strain JR2, was amplified as 3  
546 fragments with overlapping sequences (**Table S1f**). The 5' most fragment containing the  
547 promoter was amplified using primers A + B, the ORF with primers C+D, the Hyg promoter and  
548 ORF with primers E+F, and the 3' end of the CenH3 locus with primers G+H. The four fragments  
549 were combined by overlap PCR using primers A + H and cloned into a *Psp*OMI and *Sph*I  
550 linearized vector using Gibson Assembly. The vector construction was confirmed by Sanger  
551 sequencing. Vectors were transformed to *Verticillium* with *Agrobacterium*-mediated  
552 transformation (80). Correct homologous recombination and replacement at the *CenH3* locus was  
553 verified by PCR amplification using primer I+J (**Fig. S1b, Table S1f**). Correct translation of the  
554 recombinant protein was assessed using Western analyses with anti-FLAG antibody (**Fig. S1c**).  
555 Briefly, proteins were extracted from 5-day old cultures grown in 100 ml Potato Dextrose Broth  
556 at 22°C with continuous shaking at 120 rpm. Mycelium was collected by straining over a double

557 layer of miracloth and subsequently snap-frozen in liquid nitrogen and ground with a mortar and  
558 pestle using liquid nitrogen. Approximately 0.3 g of ground mycelium was resuspended in 600  
559  $\mu$ L protein extraction buffer (50 mM HEPES pH 7.5, 150 mM NaCl, 1 mM EDTA, 1% glycerol,  
560 0.02% NP-40, 2 mM Phenylmethanesulfonyl fluoride (PMSF), 100  $\mu$ M Leupeptin, 1  $\mu$ g/mL  
561 Pepstatin), briefly vortexed, incubated on ice for 15 min and centrifuged at 4°C at 8,000 g for 3  
562 min. The supernatant was collected by transferring 20  $\mu$ L to a new tube to serve as the input  
563 control and the remaining ~500  $\mu$ L was transferred to a fresh microcentrifuge tube with 15  $\mu$ L of  
564 Anti-FLAG M2 affinity gel (catalog number A2220, Sigma-Aldrich, St. Louis, Missouri, United  
565 States) and incubated while rotating at 4°C for 1 h. Samples were centrifuged at 5,000 g, 4°C for  
566 3 min, after which the supernatant was discarded. Samples were washed with 500  $\mu$ L of lysis  
567 buffer, and the centrifugation and washing were repeated three times. Protein was eluted from the  
568 resin by adding 15  $\mu$ L of lysis buffer, 20  $\mu$ L of 2x Laemmli loading buffer (4% SDS, 20%  
569 glycerol, 0.004% bromophenol blue, 125 mM Tris HCL pH 6.8) and boiled at 95°C for 3 min.  
570 Protein samples were separated on a 12% polyacrylamide gel, and subsequently transferred to  
571 PVDF membranes, blocked in 5% BSA, washed twice in TBST, and incubated with 1:3500 anti-  
572 FLAG antibody (monoclonal anti-FLAG M2; Merck KGaA, Darmstadt, Germany).

573

#### 574 **Chromatin immunoprecipitation followed by high-throughput sequencing (ChIP-seq)**

575 For each *V. dahliae* genotype, one million spores were added to 100 ml Potato Dextrose Broth  
576 and incubated for 7 days at 22°C with continuous shaking at 120 rpm. Mycelium was collected by  
577 straining over a double layer of miracloth and subsequently snap-frozen in liquid nitrogen and  
578 ground with a mortar and pestle using liquid nitrogen. All ground material (0.5-1 gram per  
579 sample) was resuspended in 4 mL ChIP Lysis buffer (50 mM HEPES-KOH pH7.5, 140 mM  
580 NaCl, 1 mM EDTA, 1% Triton X-100, 0.1% NaDOC) and dounced 40 times in a 10 cm<sup>3</sup> glass  
581 tube with tightly fitting pestle on 800 power with a RZR50 homogenizer (Heidolph, Schwabach,  
582 Germany), followed by five rounds of 20 seconds sonication on ice with 40 seconds of resting in

583 between rounds with a Soniprep 150 (MSE, London, UK). Samples were redistributed to 2 mL  
584 tubes and pelleted for 2 min at maximum speed in a tabletop centrifuge. Supernatants were  
585 pooled per sample in a 15 mL tube together with 25  $\mu$ L  $\alpha$ -FLAG M2 magnetic beads (Sigma-  
586 Aldrich, St. Louis, Missouri, United States), incubated overnight at 4°C and continuous rotation.  
587 Beads were captured on a magnetic stand and washed with wash buffer (50 mM Tris HCl pH 8, 1  
588 mM EDTA, 1% Triton X-100, 100 mM NaCl), high-salt wash buffer (50 mM Tris HCl pH 8, 1  
589 mM EDTA, 1% Triton X-100, 350 mM NaCl), LiCl wash buffer (10 mM Tris HCl pH8, 1 mM  
590 EDTA, 0.5% Triton X-100, 250 mM LiCl), and TE buffer (10 mM Tris HCl pH 8, 1mM EDTA).  
591 Chromatin was eluted twice from beads by addition of 100  $\mu$ L pre-heated TES buffer (100 mM  
592 Tris HCl pH 8, 1% SDS, 10 mM EDTA, 50 mM NaCl) and 10 minutes incubation at 65°C. 10  
593 mg/mL 2  $\mu$ L Proteinase K was added and incubated at 65°C for 5 hours, followed chloroform  
594 extraction. DNA was precipitated by addition of 2 volumes 100% ethanol, 1/10<sup>th</sup> volume 3 M  
595 NaOAc pH 5.2 and 1/200<sup>th</sup> volume 20mg/mL glycogen, and overnight incubation at -20°C.

596 Sequencing libraries were prepared using the TruSeq ChIP Library Preparation Kit  
597 (Illumina, city, country) according to the manufacturer's instructions, but without gel purification  
598 and with use of the Velocity DNA Polymerase (BioLine, Luckenwalde, Germany) for 12 cycles  
599 of amplification for the FLAG-CenH3. H3K4me2 ChIP was performed as described previously  
600 (36), using an  $\alpha$ -H3K4me2 antibody (#39913, ActiveMotif; Carlsbad, California, United States).  
601 Single-end (125 bp) sequencing was performed on the Illumina HiSeq2500 platform at KeyGene  
602 N.V. (Wageningen, the Netherlands).

603

#### 604 **Chromatin confirmation capturing followed by high-throughput sequencing (Hi-C)**

605 We determined the inter- and intra-chromosomal contact frequencies using Hi-C in *V. dahliae*  
606 strains CQ2, JR2, and VdLs17, as well as in *V. albo-atrum* strain PD747, *V. alfalfae* strain  
607 PD683, *V. isaacii* strain PD618, *V. klebahnii* strain PD401, *V. longisporum* strain PD589, *V.*

608 *nonalfalae* strain T2, *V. nubilum* strain 397, *V. tricorpus* strain PD593, and *V. zaregamsianum*  
609 strain PD739. For each strain, one million spores were added to 400 mL Potato Dextrose Broth  
610 and incubated for 6 days at 22°C with continuous shaking at 120 rpm. Mycelium was collected by  
611 straining over double layer miracloth and 300 mg (fresh weight) was used as input for generating  
612 Hi-C sequencing libraries with the Proximo Hi-C kit (Microbe) (Phase Genomics, Seattle, WA,  
613 USA), according to manufacturer's instructions. Hi-C sequencing libraries of *V. dahliae* strains  
614 CQ2, JR2. and VdLs17 were paired end (2x125 bp) sequenced on the Illumina HiSeq2500  
615 platform at KeyGene N.V. (Wageningen, the Netherlands). Hi-C sequencing libraries of the other  
616 *Verticillium* species were paired-end (2x150 bp) sequenced on the NextSeq500 platform at USEQ  
617 (Utrecht, the Netherlands).

618

#### 619 ***In vitro* transcriptome profiling using RNA-seq**

620 RNA sequencing of *V. albo-atrum* strain PD747, *V. isaacii* strain PD618, *V. klebahnii* strain  
621 PD401, *V. longisporum* strain PD589, *V. nonalfalae* strain T2, *V. nubilum* strain 397, *V.*  
622 *tricorpus* strain PD593, and *V. zaregamsianum* strain PD739 as described previously (36). Single-  
623 end (50 bp) sequencing was performed on the BGISEq500 platform at BGI (BGI Hong Kong).

624

#### 625 **Analyses of high-throughput sequencing data**

626 High-throughput sequencing libraries (**Table S1a**) have been analyzed as follows: Illumina reads  
627 were quality-filtered and trimmed using trimmomatic (version 0.36) (81). Sequencing reads were  
628 trimmed and filtered by removing Illumina TruSeq sequencing adapters (settings seed  
629 mismatches 2, palindrome clip threshold 30, and simple clip threshold 10), removal of low-  
630 quality leading or trailing bases below quality 5 and 10, respectively, and 4-base sliding window  
631 trimming and cutting when average quality per base dropped below 15. Additionally, filtered and  
632 trimmed reads < 90 nt were removed from further analyses. Filtered and trimmed reads were  
633 mapped to the corresponding genome assembly with Bowtie2 (default settings) (82), and mapping



634 files were converted to bam-format using samtools (v 1.8) (83). Genomic coverage was  
635 determined using deepTools (v3.4.1; bamCoverage) (84) by extending sequencing reads to 147  
636 bp followed by RPGC normalization with a bin-size of 1,000 bp and smoothing of 3,000 bp. To  
637 assess between sample variability, we used deepTools (v3.4.1, plotPCA) (84) to generate  
638 principle component analyses. Furthermore, we employed deepTools (v3.4.1,  
639 multiBigwigSummary) (84) to summarize genomic coverages of over genes, repetitive elements,  
640 and genomic windows (5 kb windows with 500 bp slide). Genomic regions enriched for FLAG-  
641 CenH3 were identified using MACS2 (v2.1.1) (broad peak option; broad cutoff 0.0025) (85).

642 To determine DNA (cytosine) methylation, we utilized sequencing data of bisulfite treated  
643 genomic DNA previously generated for *V. dahliae* strain JR2 (36). Sequencing reads were  
644 mapped to the *V. dahliae* strain JR2 genome assembly as previously described (36).  
645 Subsequently, the number of reads supporting cytosine methylation in CG-context were extracted,  
646 and weighted CG-methylation levels were calculated over genes, repetitive elements, and  
647 genomic windows (5 kb window size with 500 bp slide) (86); weighted CG-methylation was  
648 defined as the sum of reads supporting cytosine methylations divided by the sum of all reads  
649 occurring at all CG sites in the respective regions. Sites with less than four reads were not  
650 considered.

651 To improve the genome assemblies of the *Verticillium* species, we mapped Hi-C  
652 sequencing reads to genome assemblies of *V. dahliae* strain CQ2, *V. albo-atrum* strain PD747, *V.*  
653 *alfalfae* strain PD683, *V. isaacii* strain PD618, *V. klebahnii* strain PD401, *V. longisporum* strain  
654 PD589, *V. nonalfalfae* strain T2, *V. nubilum* strain 397, *V. tricorpus* strain PD593, and *V.*  
655 *zaregamsianum* strain PD739 using Juicer (v1.6) with early stage setting (87). The contact  
656 matrices generated by juicer were used by the 3D de novo assembly (3D-DNA) pipeline (88)  
657 (v180922) with a contig size threshold of 1000bp to eliminate mis-joints in the previous  
658 assemblies and to generate improved assemblies. The genome assemblies were manually

659 improved using Juicebox Assembly Tools (JBAT) (v1.11.08) (89) and improved genome  
660 assemblies were generated using the 3D-DNA post-review asm pipeline (88). Centromere  
661 locations were determined using a 1 kb-resolution contact matrix in JBAT, by identifying a region  
662 per chromosome that displays strong inter-chromosomal interactions, yet weak intra-  
663 chromosomal interactions (see Figure S12, S13).

664 To assess potential repeat collapses during genome assemblies at centromeric regions, we  
665 mapped previously generated short-read data *V. dahliae* strain JR2 and VdLs17, *V. albo-atrum*  
666 strain PD747, *V. alfalfae* strain PD683, *V. isaacii* strain PD618, *V. klebahnii* strain PD401, *V.*  
667 *longisporum* strain PD589, *Verticillium nonalfalfae* strain T2, *V. tricorpus* strain PD593, and *V.*  
668 *zaregamsianum* strain PD739 (39, 40, 90, 91) to the genome assemblies using BWA (v0.7.17;  
669 mem) (83). We first used bedtools (v2.29.2) (92) to identify few genomic regions with > 500x  
670 coverage. We then applied deepTools (v3.4.1, computeGCBias) (84) to compute GC biases of  
671 read depth across the genome, excluding the identified high coverage regions, and used  
672 deepTools (v3.4.1, correctGCBias) (84) to correct GC biases, which addresses known biases in  
673 sequencing library preparation to ensure even read coverage throughout the genome irrespective  
674 of their base composition (93). We used deepTools (v3.4.1, bamCoverage, bins 50 bp, CPM  
675 normalization) (84) to obtain the read coverage throughout the genome, excluding regions  
676 containing sequence assembly gaps (Ns). Assuming that collapsed repeats would lead to a local  
677 increase in read depth, we used the ratio of the average read coverage at the centromeres and  
678 outside of the centromere at each chromosome to correct the inferred centromere sizes. To further  
679 validate the genome assembly of regions identified as centromeres of *V. dahliae* strain JR2, the  
680 genome assembly was compared to the previously generated optical map (35) using MapSolver (v  
681 3.2; OpGen, Gaithersburg, MD).

682 The transcriptional activity for genes and repetitive elements in *V. dahliae* strain JR2 was  
683 assessed *in vitro* (in Potato Dextrose Broth) using previously generated deep transcriptome

684 datasets (36). To this end, single-end sequencing reads of three biological replicates were mapped  
685 to the *V. dahliae* strain JR2 genome assembly (32) using STAR (v2.4.2a; max. intron size 1 kb  
686 and outFilterMismatchNmax to 5) (94). The resulting mapped reads were summarized per  
687 genomic feature (gene or repeat) using summarizeOverlaps (95), converted to counts per million  
688 (cpm) mapped reads, and averaged over the three biological replicates.

689

### 690 **Sequence analyses of *Verticillium* genome assemblies, centromeres, repeat and gene content**

691 Repetitive elements in the genomes of *V. dahliae* strains JR2, VdLs17 and CQ2 (32, 33) were  
692 identified as previously described (36). Briefly, repetitive elements were identified in each  
693 genome independently using a combination of LTRharvest (96) and LTRdigest (97) followed by  
694 identification of RepeatModeler. Identified repeats in the different *V. dahliae* strains were  
695 clustered into a non-redundant library that contained consensus sequences for each repeat family.  
696 The repeat library was manually curated and annotated using PASTEC (98) or by sequence  
697 similarity to previously identified and characterized repeat families (32, 44). Genome-wide  
698 occurrences of repeat families were determined using RepeatMasker (v 4.0.9; sensitive option and  
699 cutoff 250), and the output was postprocessed using ‘One code to find then all’ (99). We only  
700 considered matches to the repeat consensus library, and thereby excluded simple repeats and low-  
701 complexity regions.

702 *De novo* gene and repeat annotation for the Hi-C-improved *Verticillium* genome  
703 assemblies, and for *V. dahliae* strains JR2 and VdLs17 as a comparison was performed using the  
704 funannotate pipeline (100). Briefly, repetitive elements were first *de novo* identified using  
705 RepeatModeler and masked for gene prediction using RepeatMasker. Subsequently, gene  
706 prediction parameters were estimated using *in vitro* RNA-seq data (see above for details;  
707 exception: *V. alfalfae* for which no RNA-seq data was available, *V. nonalfalfae* for which  
708 publicly available RNA-seq data was used (90), and *V. dahliae* strain JR2 for which in addition to

709 the *in vitro* RNA-seq data generated in this study, also previously generated *in vitro* (xylem sap  
710 and half-MS; (36)) as well as long-read nanopore cDNA data (101) was used). Based on the gene  
711 prediction parameters, gene prediction was performed with funannotate using a combination of *ab*  
712 *initio* gene predictors, consensus predictions were obtained using Evidencemodeler (v1.1.1)  
713 (102), and gene predictions were adjusted using information from the RNA-seq data. Repeat  
714 annotation for each genome assembly was based on the *de novo* repeat family consensus  
715 sequences obtained with funannotate. Genome-wide occurrences of these repeat families as well  
716 as previously defined repeat families for *V. dahliae* (see above) were determined using  
717 RepeatMasker (v 4.0.9; sensitive option and cutoff 250), and the output was postprocessed using  
718 ‘One code to find then all’ (99). *De novo* repeat families overlapping with centromeres in the  
719 different species were clustered using BLASTClust (v2.2.26; parameter ‘-S 60 -L 0.55 -b F -p F’),  
720 and subsequently visualized using Cytoscape (v.3.8.0) (103). Next to RepeatMasker, genome-  
721 wide occurrences of the previously determined *VdLTRE9* (32, 36) were identified by BLAST  
722 searches (blastn v2.9.0+; e-value cutoff 1e-5, no soft-masking and dust, fixed database size 10e6)  
723 (74, 75), and similarity between *VdLTRE9* consensus sequences and the *de novo* predicted repeat  
724 families was established using BLAST (blastn, e-value cutoff 1e-5, query coverage > 50%, no  
725 soft-masking and dust, fixed database size 10e6).

726 Repeat and gene density (*V. dahliae* strain JR2 and *VdLs17* based on previous gene  
727 annotation (101)), GC-content, and composite RIP index were calculated along the genome  
728 sequence using sliding windows (5 kb window with 500 bp slide). The composite RIP index  
729 (CRI) was calculated according to Lewis et al. (45). CRI was determined by subtracting the RIP  
730 substrate from the RIP product index, which are defined by dinucleotide frequencies as follows:  
731 RIP product index = TpA / ApT and the RIP substrate index = (CpA + TpG)/(ApC + GpT).  
732 Overlaps between different genomic features (for example repetitive elements over centromeric

733 regions) was assessed using bedtools (v2.29.2) (92). Genome-wide data was visualized using R  
734 (104) with the packages ggplot2 (105), karyplotR (106), or Gviz (107), as well as EasyFig (108).

735 Whole-genome alignments between *V. dahliae* strains JR2, VdLs17, and CQ2 were  
736 performed using NUCmer, which is part of the MUMmer package (v 3.1; --maxmatch) (109). To  
737 remove short matches, we only considered alignments longer than 10 kb. Ancestral genome  
738 configurations were reconstructed using AnChro (56). We first determined the synteny  
739 relationships between all possible pairs of haploid *Verticillium* genomes and two outgroup  
740 genomes (*Plectosphaerella cucumerina* and *Sodiomyces alkalinus*) using SynChro with synteny  
741 block stringency (delta parameter) ranging from 2-5 (110). We then obtained all ancestors by  
742 calculating all possible pairs of genomes (G1 and G2) and outgroups (G3,...,G<sub>n</sub>) and by varying  
743 the delta' (G1 and G2 comparisons) and delta'' (G1/G3..G1/G<sub>n</sub> and G2/G3..G2/G<sub>n</sub> comparisons)  
744 parameters for AnChro. We additionally reconstructed all ancestors starting from the extent  
745 genomes in a sequential approach with multiple successive cycles of SynChro and AnChro (delta  
746 parameters varied between 2-5). For each ancestor, we chose the optimal reconstructed by the  
747 delta parameter combination (delta' and delta'') that minimizes the number of reconstructed  
748 chromosomes and rearrangements and at the same time maximizes the number of genes, both  
749 guided by the most commonly observed number of chromosomes and genes in all  
750 rearrangements. We obtained the number of large-scale rearrangements between reconstructed  
751 ancestral genomes and the extent *Verticillium* genomes using ReChro with a delta parameter of 1  
752 (56). The relationship between chromosomes of the reconstructed ancestors and the extent species  
753 in relationship to the common ancestor is generated with SynChro with a delta parameter of 1  
754 (110). A species phylogeny that uses synteny relationships computed by SynChro (see above) as  
755 informative character between the *Verticillium* genomes and the outgroup genomes was  
756 reconstructed using PhyChro (111).

757

758 **Data availability**

759 ChIP-seq and Hi-C data were submitted to the Short Read Archive (SRA) under the accession  
760 PRJNA641329 (**Table S1a**).

761

762 **ACKNOWLEDGMENTS**

763 Work in the laboratories of M.F.S and B.P.H.J.T. is supported by the Research Council Earth and  
764 Life Sciences (ALW) of the Netherlands Organization of Scientific Research (NWO).  
765 Furthermore, B.P.H.J.T. would like to acknowledge the Deutsche Forschungsgemeinschaft (DFG,  
766 German Research Foundation) under Germany's Excellence Strategy – EXC 2048/1 – Project ID:  
767 390686111. This work was supported in part by a European Molecular Biology Organization  
768 postdoctoral fellowship (EMBO, ALTF 969-2013) and Human Frontier Science Program  
769 Postdoctoral Fellowship (HFSP, LT000627/2014-L) to D.E.C. A portion of the work was also  
770 carried out in the laboratory of D.E.C. under USDA-NIFA-PBI grant 2018-67013-28492. We  
771 thank Utrecht Sequencing Facility for providing sequencing service and data. Utrecht Sequencing  
772 Facility is subsidized by the University Medical Center Utrecht, Hubrecht Institute, Utrecht  
773 University, and The Netherlands X-omics Initiative (NWO project 184.034.019).

774 **SUPPLEMENTARY MATERIAL**

775 **Figure S1** – (a) Phylogenetic analyses of the canonical H3 and the centromeric-specific CenH3 in  
776 *Verticillium dahliae* (strain JR2) and other fungal genomes. (b-c) Transformation of the coding  
777 sequence of N-terminally FLAG-tagged CenH3 directed by its native promoter at the *CenH3*  
778 locus in *Verticillium dahliae* strain JR2. (b) Correct homologous recombination and replacement  
779 at the *CenH3* locus was verified by PCR amplification was assessed using PCR and (c) Correct  
780 translation of the recombinant protein was assessed using Western Blot analyses with anti-FLAG  
781 antibody. (d) Sequencing read coverage (RPGC normalization in 1 kb bins with 3 kb  
782 smoothing) from ChIP-seq experiments using FLAG-tag antibodies on two independent  
783 transformants of *Verticillium dahliae* strain JR2 that express FLAG-tagged CenH3 and the wild-  
784 type strain are mapped to the eight chromosomes of *V. dahliae* strain JR2 (32). Gene (red) and  
785 repeat (blue) density are shown below each chromosome. (e) Principal component analysis of the  
786 four FLAG-tag ChIP-seq samples (two wild-type and two CenH3-FLGA). (f) Comparison of the  
787 centromeric regions with the identified centromeres highlighted as blue block in the genome  
788 assembly of *Verticillium dahliae* strain JR2 with a previously generated optical map (35). Vertical  
789 lines display corresponding (*in silico*) restriction sites and their alignment.

790 **Figure S2** – Schematic overview of the eight chromosomes of *Verticillium dahliae* strain JR2  
791 displaying different heterochromatin-associated chromatin modifications (mC, H3K9me3, and  
792 H3K27me3) in relation to the centromeres. The different lanes display the CenH3-FLAG ChIP-  
793 seq read coverage (RPGC normalization in 1 kb bins with 3 kb smoothing), the repeat-density,  
794 the GC-content, the CRI as well as the weighted cytosine methylation (all summarized in 5 kb  
795 windows with 500 bp slide), and the normalized H3K9me3 and H3K27me3 ChIP-seq read  
796 coverage (RPGC normalization in 1 kb bins with 3 kb smoothing).

797

798 **Figure S3** – (a) Boxplot displaying the composite RIP index (CRI) of C to T in CA recorded in  
799 genomic windows (5 kb, 500 bp slide), per gene, per annotated repeat, and per window  
800 overlapping with the CenH3-enriched centromeres. Statistical differences for the indicated  
801 comparisons were calculated using the one-sided non-parametric Mann-Whitney test; p-values <  
802 0.001: \*\*\*. (b) Summary of H3K4me2 (green), H3K9me3 (red), and H3K27me3 (orange)  
803 normalized ChIP-seq read coverage (RPGC normalization in 1 kb bins and 3 kb smoothing) in  
804 genomic bins (2.5%) across the chromosomal arms of the eight chromosomes of *Verticillium*  
805 *dahliae* strain JR2 (divided into 2.5% bins) and the centromeric regions (divided into 10% bins).  
806 The dots indicate the average ChIP-seq coverage and the whiskers indicate  $\pm 1.5$  times the  
807 interquartile range. (c-e) Boxplots displaying the (c) weighted methylation levels (CG context),  
808 (d) the composite RIP index, and (e) the expression in PDB growth medium (counts per million)  
809 for repetitive elements belonging to ten repeat families identified in the eight centromeres in  
810 *Verticillium dahliae* JR2.

811 **Figure S4 (a-c)** Whole-genome alignments between the eight chromosomes of (a) *Verticillium*  
812 *dahliae* strains JR2 and VdLs17 (32), (b) *V. dahliae* strains CQ2 and JR2 (32, 33), and (c) *V.*  
813 *dahliae* strains CQ2 and VdLs17 (32, 33). (d-e) Schematic overview of the genome assemblies of  
814 *Verticillium dahliae* strains (d) VdLs17 and (e) CQ2. The individual lanes show the GC content,  
815 the gene (red) and repeat (blue) density (all summarized in 5 kb windows with 500 bp slide), and  
816 the location of the centromere associated *VdLTRE9*. (f) Synteny analyses of the eight  
817 chromosomes of *V. dahliae* strains JR2 and CQ2. Schematic overview of the eight chromosomes  
818 of *V. dahliae* strain JR2 (left) and the corresponding syntenic regions in *V. dahliae* strains CQ2  
819 (right). Centromeres are indicated by stars, and syntenic centromeres of *V. dahliae* strain CQ2 are  
820 colored according to *Cen1-8* of *V. dahliae* strain JR2.

821 **Figure S5**– Hi-C contact matrix showing the interaction frequencies between genomic regions in  
822 (a) *V. nonalfalfae* (T2), (b) *V. alfalfae* (PD683), (c) the allodiploid *V. longisporum* (PD589), (d)



823 *V. nubilum* (397), (e) *V. albo-atrum* (PD747), (f) *V. zaregamsianum* (PD739), (g) *V. tricorpus*  
824 (PD593), (h) *V. klebhanii* (PD401), and (i) *V. isaacii* (PD618). Regions of high inter-  
825 chromosomal interaction frequencies are indicative of centromeres and are highlighted by arrow  
826 heads, and the blue line indicated boundaries between the pseudo-chromosomes.

827 **Figure S6 – (a-b)** Comparison of normalized read coverage and corrected centromere lengths for  
828 *Verticillium* species for which short-read data is available. (a) Counts per million mapped reads  
829 (CPM) normalized read coverage was calculated for GC-biased corrected short-read libraries in  
830 50 bp genomic windows, excluding regions containing assembly gaps (Ns). Genomic windows  
831 are summarized in boxplots (outliers not shown) by genomic location, centromeric regions (*Cen*,  
832 blue) and non-centromeric regions (non-*Cen*, grey). (b) Centromeric lengths inferred by Hi-C  
833 data were ‘corrected’ based on the ratio of normalized read depth between centromeres and non-  
834 centromeric regions per chromosomes. Differences for each species compared to the overall mean  
835 were computed using unpaired T-tests; p-values < 0.0001: \*\*\*\*, p-values < 0.001: \*\*\*, p-values  
836 < 0.01: \*\*, p-values < 0.05: \*. (c) The number of BLASTn matches of the *VdLTRE9* consensus  
837 element to the genomes of the *Verticillium* species separated by their genomic location,  
838 centromeric regions (*Cen*, blue) and non-centromeric regions (non-*Cen*, grey). The overall  
839 number of base pairs (bp) covered by the BLASTn matches in each genome sequence is  
840 indicated. The asterisk denotes the high number of *VdLTRE9* matches to unassigned, non-*Cen*  
841 regions in the genome assembly of *Verticillium nonalfalfae* (T2). (d) The number of repetitive  
842 element matches identified by RepeatMasker for each *Verticillium* species based on  
843 species/strain-specific repeat libraries generated by RepeatModeler separated by their genomic  
844 location, centromeric regions (*Cen*, blue) and non-centromeric regions (non-*Cen*, grey). (e) GC-  
845 content of the *Verticillium* genomes in 50 bp windows and separated by their genomic location,  
846 centromeric regions (*Cen*, blue) and non-centromeric regions (non-*Cen*, grey). (f) The repeat

847 content of centromeric regions in percent covered sequences in the different *Verticillium* species.

848 Each data point summarized in the boxplot is the repeat content per centromere.

849 **Figure S7** – Schematic overview of the centromeric regions (250 kb) in (a) *Verticillium dahliae*

850 strain JR2, in (b) species belonging to clade Flavnonexudans, and in (c) species belonging clade

851 Flavexudans. The centromeres are indicated by dark grey bars. The predicted genes (black) and

852 repeats (blue) are shown below each centromere, and location of *VdLTRE9* (partial) matches

853 (light green) are shown above each centromere. Repeats that share sequence similarity (BLASTn)

854 to the *VdLTRE9* consensus sequence are shown above each centromere (dark green).

855 **Figure S8** – Sequence comparisons of *de novo* repeat families identified with RepeatModeler and

856 RepeatMasker in the genome assemblies of the different *Verticillium* species. Individual repeat

857 family consensus sequences were clustered using BLASTClust. (a) Relationships between

858 different repeat family consensus sequences are displayed as connected graphs. The sub-graph

859 with the consensus sequences with similarity to *VdLTRE9* is highlighted in yellow. (b) The

860 presence/absence matrix indicates the occurrences of different repeat families in the analyzed

861 *Verticillium* species (black present, white absent). The cluster containing consensus sequences

862 with similarity to *VdLTRE9* is highlighted.

863 **Figure S9** – Reconstruction of ancestral genomes within the genus *Verticillium* with AnChro

864 (56). The number of (a) chromosomes and (b) genes predicted by all potential ancestral

865 reconstructions using different combinations of genomes and stringency parameters. The

866 phylogenetic tree in (a) depicts the relationships between *Verticillium* species and the

867 abbreviations used for the ancestors. The inlays display boxplots to summarize the number of (a)

868 chromosomes and (b) genes per ancestral reconstruction. (c) The number of chromosomes and

869 genes of the chosen ‘optimal’ reconstruction for each of the internal ancestors. (d) The number of

870 genes per chromosome for each of the reconstructed ancestor and the extant *Verticillium* species.

871 The star highlights the reconstruction for the B1 ancestor that had ten chromosomes, but with two

872 chromosomes with six and two genes. (e) Reconstruction of the *Verticillium* species phylogeny  
873 based on synteny relationship using PhyChro (111).

874

875 **Table S1** – (a) Overview of the different *Verticillium* sequencing libraries used in this study. (b)  
876 Position of the individual centromeric regions inferred by Hi-C inter-chromosomal interaction  
877 frequencies and the overlap (in kb) with CenH3-enriched regions and the centromere associated  
878 *VdLTRE9* in *Verticillium dahliae* JR2, VdLs17, and CQ2. (c) Overview of the different  
879 *Verticillium* genomes assembled using Hi-C interactions. (d) Position, length, and number of  
880 assembly gaps (Ns) of the individual centromeric regions inferred by Hi-C inter-chromosomal  
881 interaction in *Verticillium nonalfalfae* (T2), *Verticillium alfalfae* (PD683), the allodiploid  
882 *Verticillium longisporum* (PD589), *Verticillium nubilum* (397), *Verticillium albo-atrum* (PD747),  
883 *Verticillium zaregamsianum* (PD739), *Verticillium tricorpus* (PD593), *Verticillium klebhanii*  
884 (PD401), and *Verticillium isaacii* (PD618). (e) The number of *de novo* repeat consensus  
885 sequences identified within and outside of centromeric regions in the *Verticillium* species. Only  
886 consensus elements with > 5 matches in centromeric regions are displayed. Note that the  
887 consensus names between species/strains are not comparable. (f) The primers used for cloning the  
888 CenH3 FLAG tag in *Verticillium dahliae* strain JR2

889

890 **REFERENCES**

- 891 1. Roy B, Sanyal K. 2011. Diversity in requirement of genetic and epigenetic factors for  
892 centromere function in fungi. *Eukaryotic cell* 10:1384-1395.
- 893 2. Foley EA, Kapoor TM. 2013. Microtubule attachment and spindle assembly checkpoint  
894 signalling at the kinetochore. *Nature reviews Molecular cell biology* 14:25-37.
- 895 3. Burrack LS, Berman J. 2012. Flexibility of centromere and kinetochore structures. *Trends*  
896 *in Genetics* 28:204-212.
- 897 4. Janssen A, van der Burg M, Szuhai K, Kops GJPL, Medema RH. 2011. Chromosome  
898 segregation errors as a cause of DNA damage and structural chromosome aberrations. *Science*  
899 *(New York, NY)* 333:1895-1898.
- 900 5. Sheltzer JM, Blank HM, Pfau SJ, Tange Y, George BM, Humpton TJ, Brito IL, Hiraoka  
901 Y, Niwa O, Amon A. 2011. Aneuploidy drives genomic instability in yeast. *Science (New York,*  
902 *NY)* 333:1026-1030.
- 903 6. Barra V, Fachinetti D. 2018. The dark side of centromeres: Types, causes and  
904 consequences of structural abnormalities implicating centromeric DNA. *Nature Communications*  
905 9:4340.
- 906 7. Seidl MF, Thomma BPHJ. 2014. Sex or no sex: Evolutionary adaptation occurs  
907 regardless. *BioEssays* 36:335-345.
- 908 8. Faino L, Seidl MF, Shi-Kunne X, Pauper M, van den Berg GCM, Wittenberg AHJ,  
909 Thomma BPHJ. 2016. Transposons passively and actively contribute to evolution of the two-  
910 speed genome of a fungal pathogen. *Genome Research* 26:1091-1100.
- 911 9. Rancati G, Pavelka N, Fleharty B, Noll A, Trimble R, Walton K, Perera A, Staehling-  
912 Hampton K, Seidel CW, Li R. 2008. Aneuploidy underlies rapid adaptive evolution of yeast cells  
913 deprived of a conserved cytokinesis motor. *Cell* 135:879-893.
- 914 10. Pavelka N, Rancati G, Zhu J, Bradford WD, Saraf A, Florens L, Sanderson BW, Hattem  
915 GL, Li R. 2010. Aneuploidy confers quantitative proteome changes and phenotypic variation in  
916 budding yeast. *Nature* 468:321-325.

- 917 11. Sankaranarayanan SR, Ianiri G, Coelho MA, Reza MH, Thimmappa BC, Ganguly P,  
918 Vadnala RN, Sun S, Siddharthan R, Tellgren-Roth C, Dawson TLJ, Heitman J, Sanyal K. 2020.  
919 Loss of centromere function drives karyotype evolution in closely related *Malassezia* species.  
920 *Elife* 9.
- 921 12. Ola M, O'Brien CE, Coughlan AY, Ma Q, Donovan PD, Wolfe KH, Butler G. 2020.  
922 Polymorphic centromere locations in the pathogenic yeast *Candida parapsilosis*. *bioRxiv*  
923 doi:10.1101/2020.04.09.034512:2020.04.09.034512.
- 924 13. Yadav V, Sreekumar L, Guin K, Sanyal K. 2018. Five pillars of centromeric chromatin in  
925 fungal pathogens. *PLoS pathogens* 14:e1007150.
- 926 14. Henikoff S, Ahmad K, Malik HS. 2001. The centromere paradox: Stable inheritance with  
927 rapidly evolving DNA. *Science* 293:1098-102.
- 928 15. Smith KM, Galazka JM, Phatale PA, Connolly LR, Freitag M. 2012. Centromeres of  
929 filamentous fungi. *Chromosome research : an international journal on the molecular,*  
930 *supramolecular and evolutionary aspects of chromosome biology* 20:635-656.
- 931 16. Yadav V, Sun S, Billmyre RB, Thimmappa BC, Shea T, Lintner R, Bakkeren G, Cuomo  
932 CA, Heitman J, Sanyal K. 2018. RNAi is a critical determinant of centromere evolution in closely  
933 related fungi. *Proceedings of the National Academy of Sciences of the United States of America*  
934 115:3108-3113.
- 935 17. Fitzgerald-Hayes M, Clarke L, Carbon J. 1982. Nucleotide sequence comparisons and  
936 functional analysis of yeast centromere DNAs. *Cell* 29:235-244.
- 937 18. Furuyama S, Biggins S. 2007. Centromere identity is specified by a single centromeric  
938 nucleosome in budding yeast. *Proceedings of the National Academy of Sciences of the United*  
939 *States of America* 104:14706-14711.
- 940 19. Krassovsky K, Henikoff JG, Henikoff S. 2012. Tripartite organization of centromeric  
941 chromatin in budding yeast. *Proceedings of the National Academy of Sciences of the United*  
942 *States of America* 109:243-248.
- 943 20. Cliften PF, Fulton RS, Wilson RK, Johnston M. 2006. After the duplication: gene loss  
944 and adaptation in *Saccharomyces* genomes. *Genetics* 172:863-872.

- 945 21. Baum M, Sanyal K, Mishra PK, Thaler N, Carbon J. 2006. Formation of functional  
946 centromeric chromatin is specified epigenetically in *Candida albicans*. *Proceedings of the*  
947 *National Academy of Sciences of the United States of America* 103:14877-14882.
- 948 22. Padmanabhan S, Thakur J, Siddharthan R, Sanyal K. 2008. Rapid evolution of Cse4p-rich  
949 centromeric DNA sequences in closely related pathogenic yeasts, *Candida albicans* and *Candida*  
950 *dubliniensis*. *Proceedings of the National Academy of Sciences of the United States of America*  
951 105:19797-19802.
- 952 23. Sanyal K, Baum M, Carbon J. 2004. Centromeric DNA sequences in the pathogenic yeast  
953 *Candida albicans* are all different and unique. *Proceedings of the National Academy of Sciences*  
954 *of the United States of America* 101:11374-11379.
- 955 24. Cambareri EB, Aisner R, Carbon J. 1998. Structure of the chromosome VII centromere  
956 region in *Neurospora crassa*: degenerate transposons and simple repeats. *Molecular and cellular*  
957 *biology* 18:5465-5477.
- 958 25. Smith KM, Phatale PA, Sullivan CM, Pomraning KR, Freitag M. 2011. Heterochromatin  
959 is required for normal distribution of *Neurospora crassa* CenH3. *Molecular and cellular biology*  
960 31:2528-2542.
- 961 26. Selker EU. 2002. Repeat-induced gene silencing in fungi. *Advances in genetics* 46:439-  
962 450.
- 963 27. Schotanus K, Soyer JL, Connolly LR, Grandaubert J, Happel P, Smith KM, Freitag M,  
964 Stukenbrock EH. 2015. Histone modifications rather than the novel regional centromeres of  
965 *Zymoseptoria tritici* distinguish core and accessory chromosomes. *Epigenetics & Chromatin* 8:41.
- 966 28. Thomma BPHJ, Seidl MF, Shi-Kunne X, Cook DE, Bolton MD, van Kan JAL, Faino L.  
967 2016. Mind the gap; Seven reasons to close fragmented genome assemblies. *Fungal Genetics and*  
968 *Biology* 90:24-30.
- 969 29. Yadav V, Yang F, Reza MH, Liu S, Valent B, Sanyal K, Naqvi NI. 2019. Cellular  
970 dynamics and genomic identity of centromeres in cereal blast fungus. *mBio* 10.
- 971 30. Fang Y, Coelho MA, Shu H, Schotanus K, Thimmappa BC, Yadav V, Chen H, Malc EP,  
972 Wang J, Mieczkowski PA, Kronmiller B, Tyler BM, Sanyal K, Dong S, Nowrousian M, Heitman

- 973 J. 2020. Long transposon-rich centromeres in an oomycete reveal divergence of centromere  
974 features in Stramenopila-Alveolata-Rhizaria lineages. *PLoS Genetics* 16:e1008646.
- 975 31. Navarro-Mendoza MI, Perez-Arques C, Panchal S, Nicolas FE, Mondo SJ, Ganguly P,  
976 Pangilinan J, Grigoriev IV, Heitman J, Sanyal K, Garre V. 2019. Early diverging fungus *Mucor*  
977 *circinelloides* lacks centromeric histone CENP-A and displays a mosaic of point and regional  
978 centromeres. *Current Biology* 29:3791-3802 e6.
- 979 32. Faino L, Seidl MF, Datema E, van den Berg GCM, Janssen A, Wittenberg AHJ, Thomma  
980 BPHJ. 2015. Single-Molecule Real-Time sequencing combined with optical mapping yields  
981 completely finished fungal genome. *mBio* 6:e00936-15.
- 982 33. Depotter JRL, Shi-Kunne X, Missonnier H, Liu T, Faino L, van den Berg GCM, Wood  
983 TA, Zhang B, Jacques A, Seidl MF, Thomma BPHJ. 2019. Dynamic virulence-related regions of  
984 the plant pathogenic fungus *Verticillium dahliae* display enhanced sequence conservation.  
985 *Molecular Ecology* 28:3482-3495.
- 986 34. de Jonge R, van Esse PH, Maruthachalam K, Bolton MD, Santhanam P, Saber MK,  
987 Zhang Z, Usami T, Lievens B, Subbarao KV, Thomma BPHJ. 2012. Tomato immune receptor  
988 Ve1 recognizes effector of multiple fungal pathogens uncovered by genome and RNA  
989 sequencing. *Proceedings of the National Academy of Sciences of the United States of America*  
990 109:5110-5115.
- 991 35. de Jonge R, Bolton MD, Kombrink A, van den Berg GCM, Yadeta KA, Thomma BPHJ.  
992 2013. Extensive chromosomal reshuffling drives evolution of virulence in an asexual pathogen.  
993 *Genome research* 23:1271-1282.
- 994 36. Cook DE, Kramer M, Seidl MF, Thomma BP. 2020. Chromatin features define adaptive  
995 genomic regions in a fungal plant pathogen. *bioRxiv*  
996 doi:10.1101/2020.01.27.921486:2020.01.27.921486.
- 997 37. Inderbitzin P, Bostock RM, Davis RM, Usami T, Platt HW, Subbarao KV. 2011.  
998 Phylogenetics and taxonomy of the fungal vascular wilt pathogen *Verticillium*, with the  
999 descriptions of five new species. *PloS one* 6:e28341.
- 1000 38. Inderbitzin P, Davis RM, Bostock RM, Subbarao KV. 2011. The ascomycete *Verticillium*  
1001 *longisporum* is a hybrid and a plant pathogen with an expanded host range. *PloS one* 6:e18260.

- 1002 39. Depotter JRL, Beveren Fv, Rodriguez-Moreno L, van den Berg GCM, Wood TA,  
1003 Thomma BPHJ, Seidl MF. 2018. Homogenization of sub-genome secretome gene expression  
1004 patterns in the allodiploid fungus *Verticillium longisporum*. *bioRxiv*:341636.
- 1005 40. Shi-Kunne X, Faino L, van den Berg GCM, Thomma BPHJ, Seidl MF. 2018. Evolution  
1006 within the fungal genus *Verticillium* is characterized by chromosomal rearrangement and gene  
1007 loss. *Environmental Microbiology* 20:1362-1373.
- 1008 41. Depotter JRL, Seidl MF, van den Berg GCM, Thomma BPHJ, Wood TA. 2017. A  
1009 distinct and genetically diverse lineage of the hybrid fungal pathogen *Verticillium longisporum*  
1010 population causes stem striping in British oilseed rape. *Environmental Microbiology* 19:3997-  
1011 4009.
- 1012 42. Moeller M, Habig M, Lorrain C, Feurtey A, Haueisen J, Fagundes WC, Alizadeh A,  
1013 Freitag M, Stukenbrock EH. 2020. Recent loss of the Dim2 cytosine DNA methyltransferase  
1014 impacts mutation rate and evolution in a fungal plant pathogen. *bioRxiv*  
1015 doi:10.1101/2020.03.27.012203:2020.03.27.012203.
- 1016 43. Klosterman SJ, Subbarao KV, Kang S, Veronese P, Gold SE, Thomma BPHJ, Chen Z,  
1017 Henrissat B, Lee Y-H, Park J, Garcia-Pedrajas MD, Barbara DJ, Anchieta A, de Jonge R,  
1018 Santhanam P, Maruthachalam K, Atallah Z, Amyotte SG, Paz Z, Inderbitzin P, Hayes RJ, Heiman  
1019 DI, Young S, Zeng Q, Engels R, Galagan J, Cuomo CA, Dobinson KF, Ma L-J. 2011.  
1020 Comparative genomics yields insights into niche adaptation of plant vascular wilt pathogens.  
1021 *PLoS pathogens* 7:e1002137.
- 1022 44. Amyotte SG, Tan X, Pennerman K, del Mar Jimenez-Gasco M, Klosterman SJ, Ma L-J,  
1023 Dobinson KF, Veronese P. 2012. Transposable elements in phytopathogenic *Verticillium* spp.:  
1024 insights into genome evolution and inter- and intra-specific diversification. *BMC genomics*  
1025 13:314.
- 1026 45. Lewis ZA, Honda S, Khlafallah TK, Jeffress JK, Freitag M, Mohn F, Schubeler D, Selker  
1027 EU. 2009. Relics of repeat-induced point mutation direct heterochromatin formation in  
1028 *Neurospora crassa*. *Genome Research* 19:427-437.
- 1029 46. Liu S-Y, Lin J-Q, Wu H-L, Wang C-C, Huang S-J, Luo Y-F, Sun J-H, Zhou J-X, Yan S-  
1030 J, He J-G, Wang J, He Z-M. 2012. Bisulfite sequencing reveals that *Aspergillus flavus* holds a  
1031 hollow in DNA methylation. *PloS one* 7:e30349.



- 1032 47. Seymour M, Ji L, Santos AM, Kamei M, Sasaki T, Basenko EY, Schmitz RJ, Zhang X,  
1033 Lewis ZA. 2016. Histone H1 Limits DNA Methylation in *Neurospora crassa*. *G3* 6:1879-1889.
- 1034 48. Kursel LE, Malik HS. 2016. Centromeres. *Current Biology* 26:R487-R490.
- 1035 49. Friedman S, Freitag M. 2017. Evolving centromeres and kinetochores. *Advances in*  
1036 *Genetics* 98:1-41.
- 1037 50. Flutre T, Duprat E, Feuillet C, Quesneville H. 2011. Considering transposable element  
1038 diversification in de novo annotation approaches. *PLoS one* 6:e16526.
- 1039 51. Galazka JM, Klocko AD, Uesake M, Honda S, Selker EU, Freitag M. 2016. *Neurospora*  
1040 chromosomes are organized by blocs of importin alpha-dependent heterochromatin that are  
1041 largely independent of H3K9me3. *Genome research* doi:10.1101/gr.203182.115;gr.203182.115.
- 1042 52. Winter DJ, Ganley ARD, Young CA, Liachko I, Schardl CL, Dupont P-y, Berry D, Ram  
1043 A, Scott B, Cox MP. 2018. Repeat elements organise 3D genome structure and mediate  
1044 transcription in the filamentous fungus *Epichloë festucae*. *PLoS Genetics* 14:e1007467.
- 1045 53. Marie-Nelly H, Marbouty M, Cournac A, Flot J-F, Liti G, Parodi DP, Syan S, Guillén N,  
1046 Margeot A, Zimmer C, Koszul R. 2014. High-quality genome (re)assembly using chromosomal  
1047 contact data. *Nature Communications* 5:5695.
- 1048 54. Mizuguchi T, Fudenberg G, Mehta S, Belton J-M, Taneja N, Folco HD, FitzGerald P,  
1049 Dekker J, Mirny L, Barrowman J, Grewal SIS. 2014. Cohesin-dependent globules and  
1050 heterochromatin shape 3D genome architecture in *S. pombe*. *Nature* 516:432-435.
- 1051 55. Varoquaux N, Liachko I, Ay F, Burton JN, Shendure J, Dunham MJ, Vert J-P, Noble  
1052 WS. 2015. Accurate identification of centromere locations in yeast genomes using Hi-C. *Nucleic*  
1053 *Acids Research* 43:5331-5339.
- 1054 56. Vakirlis N, Sarilar V, Drillon G, Fleiss A, Agier N, Meyniel JP, Blanpain L, Carbone A,  
1055 Devillers H, Dubois K, Gillet-Markowska A, Graziani S, Huu-Vang N, Poirel M, Reisser C,  
1056 Schott J, Schacherer J, Lafontaine I, Llorente B, Neugeglise C, Fischer G. 2016. Reconstruction  
1057 of ancestral chromosome architecture and gene repertoire reveals principles of genome evolution  
1058 in a model yeast genus. *Genome Research* 26:918-32.

- 1059 57. Depotter JR, Deketelaere S, Inderbitzin P, Tiedemann AV, Hofte M, Subbarao KV,  
1060 Wood TA, Thomma BP. 2016. *Verticillium longisporum*, the invisible threat to oilseed rape and  
1061 other brassicaceous plant hosts. *Molecular Plant Pathology* 17:1004-16.
- 1062 58. Muller H, Gil J, Jr., Drinnenberg IA. 2019. The impact of centromeres on spatial genome  
1063 architecture. *Trends in Genetics* 35:565-578.
- 1064 59. Treangen TJ, Salzberg SL. 2011. Repetitive DNA and next-generation sequencing:  
1065 Computational challenges and solutions. *Nature Reviews Genetics* 13:36-46.
- 1066 60. Seidl MF, Faino L, Shi-Kunne X, van den Berg GCM, Bolton MD, Thomma BPHJ.  
1067 2015. The genome of the saprophytic fungus *Verticillium tricorpus* reveals a complex effector  
1068 repertoire resembling that of its pathogenic relatives. *Molecular Plant-Microbe Interactions*  
1069 28:362-373.
- 1070 61. Sun S, Yadav V, Billmyre RB, Cuomo CA, Nowrousian M, Wang L, Souciet JL,  
1071 Boekhout T, Porcel B, Wincker P, Granek JA, Sanyal K, Heitman J. 2017. Fungal genome and  
1072 mating system transitions facilitated by chromosomal translocations involving intercentromeric  
1073 recombination. *PLoS Biology* 15:e2002527.
- 1074 62. International Chicken Genome Sequencing C. 2004. Sequence and comparative analysis  
1075 of the chicken genome provide unique perspectives on vertebrate evolution. *Nature* 432:695-716.
- 1076 63. Fukagawa T. 2017. Critical histone post-translational modifications for centromere  
1077 function and propagation. *Cell Cycle* 16:1259-1265.
- 1078 64. Sullivan BA, Karpen GH. 2004. Centromeric chromatin exhibits a histone modification  
1079 pattern that is distinct from both euchromatin and heterochromatin. *Nature Structural &*  
1080 *Molecular Biology* 11:1076-83.
- 1081 65. Volpe TA, Kidner C, Hall IM, Teng G, Grewal SI, Martienssen RA. 2002. Regulation of  
1082 heterochromatic silencing and histone H3 lysine-9 methylation by RNAi. *Science* 297:1833-7.
- 1083 66. Li X, Wang X, He K, Ma Y, Su N, He H, Stolc V, Tongprasit W, Jin W, Jiang J,  
1084 Terzaghi W, Li S, Deng XW. 2008. High-resolution mapping of epigenetic modifications of the  
1085 rice genome uncovers interplay between DNA methylation, histone methylation, and gene  
1086 expression. *Plant Cell* 20:259-76.

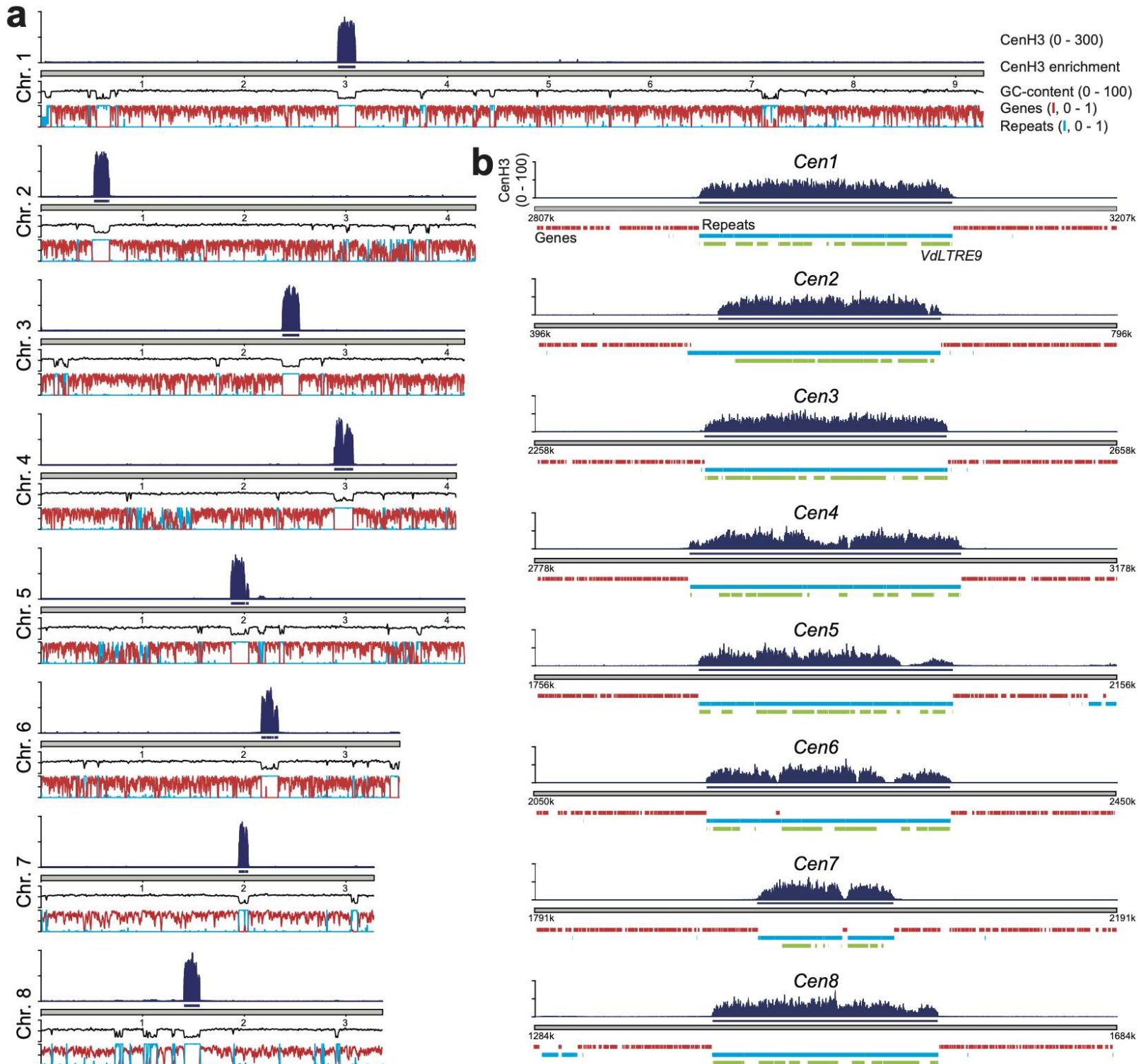
- 1087 67. Blower MD, Sullivan BA, Karpen GH. 2002. Conserved organization of centromeric  
1088 chromatin in flies and humans. *Dev Cell* 2:319-30.
- 1089 68. Lewis ZA, Adhvaryu KK, Honda S, Shiver AL, Knip M, Sack R, Selker EU. 2010. DNA  
1090 methylation and normal chromosome behavior in *Neurospora* depend on five components of a  
1091 histone methyltransferase complex, DCDC. *PLoS Genetics* 6:e1001196.
- 1092 69. Bayne EH, White SA, Kagansky A, Bijos DA, Sanchez-Pulido L, Hoe KL, Kim DU,  
1093 Park HO, Ponting CP, Rappsilber J, Allshire RC. 2010. Stc1: A critical link between RNAi and  
1094 chromatin modification required for heterochromatin integrity. *Cell* 140:666-77.
- 1095 70. Buhler M, Moazed D. 2007. Transcription and RNAi in heterochromatic gene silencing.  
1096 *Nature Structural & Molecular Biology* 14:1041-8.
- 1097 71. Yang J, Sun S, Zhang S, Gonzalez M, Dong Q, Chi Z, Chen YH, Li F. 2018.  
1098 Heterochromatin and RNAi regulate centromeres by protecting CENP-A from ubiquitin-mediated  
1099 degradation. *PLoS Genetics* 14:e1007572.
- 1100 72. Kagansky A, Folco HD, Almeida R, Pidoux AL, Boukaba A, Simmer F, Urano T,  
1101 Hamilton GL, Allshire RC. 2009. Synthetic heterochromatin bypasses RNAi and centromeric  
1102 repeats to establish functional centromeres. *Science* 324:1716-9.
- 1103 73. Jesenicnik T, Stajner N, Radisek S, Jakse J. 2019. RNA interference core components  
1104 identified and characterised in *Verticillium nonalfalfae*, a vascular wilt pathogenic plant fungi of  
1105 hops. *Scientific Reports* 9:8651.
- 1106 74. Altschul SF, Gish W, Miller W, Myers EW, Lipman DJ. 1990. Basic local alignment  
1107 search tool. *Journal of molecular biology* 215:403-410.
- 1108 75. Camacho C, Coulouris G, Avagyan V, Ma N, Papadopoulos J, Bealer K, Madden TL.  
1109 2009. BLAST+: architecture and applications. *BMC Bioinformatics* 10:421.
- 1110 76. Slater GS, Birney E. 2005. Automated generation of heuristics for biological sequence  
1111 comparison. *BMC Bioinformatics* 6:31.
- 1112 77. Katoh K, Standley DM. 2013. MAFFT multiple sequence alignment software version 7:  
1113 improvements in performance and usability. *Molecular biology and evolution* 30:772-780.

- 1114 78. Nguyen LT, Schmidt HA, von Haeseler A, Minh BQ. 2015. IQ-TREE: A fast and  
1115 effective stochastic algorithm for estimating maximum-likelihood phylogenies. *Molecular*  
1116 *Biology and Evolution* 32:268-74.
- 1117 79. Frandsen RJ, Andersson JA, Kristensen MB, Giese H. 2008. Efficient four fragment  
1118 cloning for the construction of vectors for targeted gene replacement in filamentous fungi. *BMC*  
1119 *Mol Biol* 9:70.
- 1120 80. Santhanam P. 2012. Random insertional mutagenesis in fungal genomes to identify  
1121 virulence factors. *Methods Mol Biol* 835:509-17.
- 1122 81. Bolger AM, Lohse M, Usadel B. 2014. Trimmomatic: a flexible trimmer for Illumina  
1123 sequence data. *Bioinformatics (Oxford, England)* 30:2114-2120.
- 1124 82. Langmead B, Salzberg SL. 2012. Fast gapped-read alignment with Bowtie 2. *Nature*  
1125 *methods* 9:357-359.
- 1126 83. Li H, Durbin R. 2009. Fast and accurate short read alignment with Burrows-Wheeler  
1127 transform. *Bioinformatics (Oxford, England)* 25:1754-1760.
- 1128 84. Ramirez F, Ryan DP, Gruning B, Bhardwaj V, Kilpert F, Richter AS, Heyne S, Dundar F,  
1129 Manke T. 2016. deepTools2: a next generation web server for deep-sequencing data analysis.  
1130 *Nucleic Acids Res* 44:W160-5.
- 1131 85. Zhang Y, Liu T, Meyer CA, Eeckhoute J, Johnson DS, Bernstein BE, Nusbaum C, Myers  
1132 RM, Brown M, Li W, Liu XS. 2008. Model-based analysis of ChIP-Seq (MACS). *Genome*  
1133 *Biology* 9:R137.
- 1134 86. Schultz MD, Schmitz RJ, Ecker JR. 2012. ‘Leveling’ the playing field for analyses of  
1135 single-base resolution DNA methylomes. *Trends in Genetics* 28:583-585.
- 1136 87. Durand NC, Shamim MS, Machol I, Rao SS, Huntley MH, Lander ES, Aiden EL. 2016.  
1137 Juicer Provides a One-Click System for Analyzing Loop-Resolution Hi-C Experiments. *Cell*  
1138 *Systems* 3:95-8.
- 1139 88. Dudchenko O, Batra SS, Omer AD, Nyquist SK, Hoeger M, Durand NC, Shamim MS,  
1140 Machol I, Lander ES, Aiden AP, Aiden EL. 2017. *De novo* assembly of the *Aedes aegypti*  
1141 genome using Hi-C yields chromosome-length scaffolds. *Science* 356:92-95.

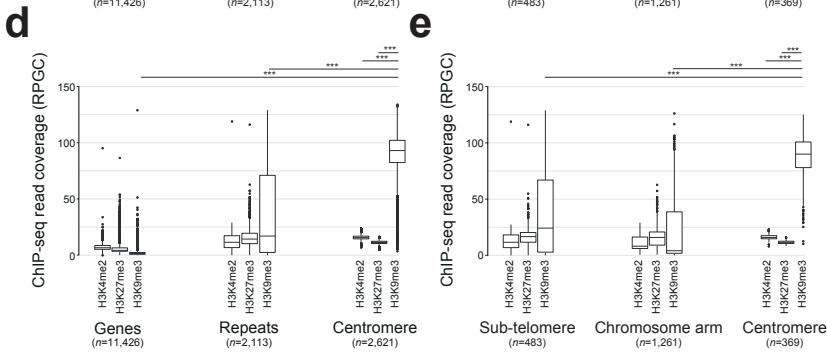
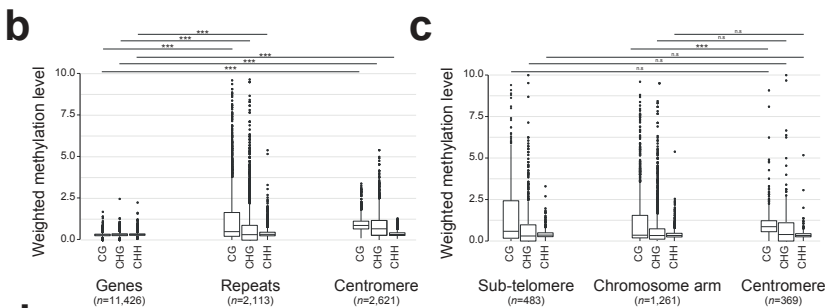
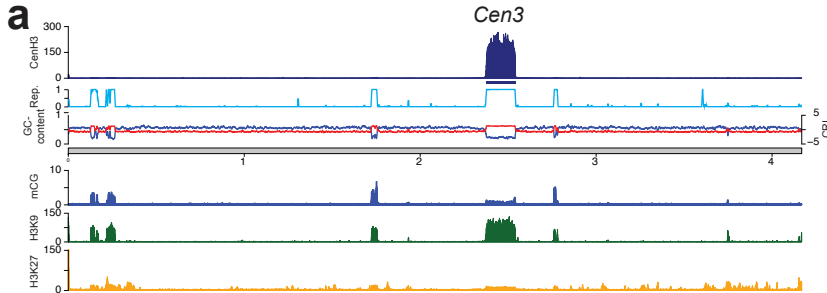
- 1142 89. Dudchenko O, Shamim MS, Batra SS, Durand NC, Musial NT, Mostofa R, Pham M,  
1143 Glenn St Hilaire B, Yao W, Stamenova E, Hoeger M, Nyquist SK, Korchina V, Pletch K,  
1144 Flanagan JP, Tomaszewicz A, McAloose D, Pérez Estrada C, Novak BJ, Omer AD, Aiden EL.  
1145 2018. The Juicebox Assembly Tools module facilitates *de novo* assembly of mammalian genomes  
1146 with chromosome-length scaffolds for under \$1000. *bioRxiv* doi:10.1101/254797:254797.
- 1147 90. Jakse J, Jelen V, Radisek S, de Jonge R, Mandelc S, Majer A, Curk T, Zupan B, Thomma  
1148 B, Javornik B. 2018. Genome sequence of a lethal strain of xylem-Invasive *Verticillium*  
1149 *nonalfalfae*. *Genome Announcements* 6.
- 1150 91. de Jonge R, Peter van Esse H, Maruthachalam K, Bolton MD, Santhanam P, Saber MK,  
1151 Zhang Z, Usami T, Lievens B, Subbarao KV, Thomma BPHJ. 2012. Tomato immune receptor  
1152 Ve1 recognizes effector of multiple fungal pathogens uncovered by genome and RNA  
1153 sequencing. *Proceedings of the National Academy of Sciences of the United States of America*  
1154 109:5110-5115.
- 1155 92. Quinlan AR, Hall IM. 2010. BEDTools: A flexible suite of utilities for comparing  
1156 genomic features. *Bioinformatics* 26:841-2.
- 1157 93. Benjamini Y, Speed TP. 2012. Summarizing and correcting the GC content bias in high-  
1158 throughput sequencing. *Nucleic Acids Research* 40:e72.
- 1159 94. Dobin A, Gingeras TR. 2015. Mapping RNA-seq reads with STAR. *Current Protocols in*  
1160 *Bioinformatics* 51:11 14 1-11 14 19.
- 1161 95. Lawrence M, Huber W, Pages H, Aboyoun P, Carlson M, Gentleman R, Morgan MT,  
1162 Carey VJ. 2013. Software for computing and annotating genomic ranges. *PLoS Computational*  
1163 *Biology* 9:e1003118.
- 1164 96. Ellinghaus D, Kurtz S, Willhoeft U. 2008. LTRharvest, an efficient and flexible software  
1165 for de novo detection of LTR retrotransposons. *BMC Bioinformatics* 9:18.
- 1166 97. Steinbiss S, Willhoeft U, Gremme G, Kurtz S. 2009. Fine-grained annotation and  
1167 classification of de novo predicted LTR retrotransposons. *Nucleic Acids Res* 37:7002-13.
- 1168 98. Hoede C, Arnoux S, Moisset M, Chaumier T, Inizan O, Jamilloux V, Quesneville H.  
1169 2014. PASTEC: an automatic transposable element classification tool. *PloS one* 9:e91929.

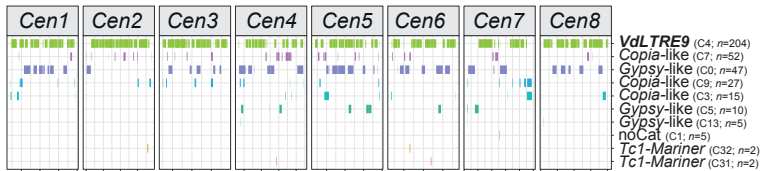
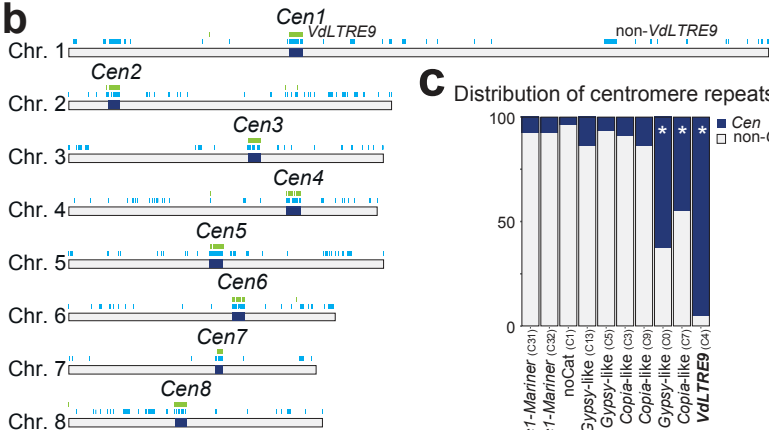
- 1170 99. Bailly-Bechet M, Haudry A, Lerat E. 2014. “One code to find them all”: a perl tool to  
1171 conveniently parse RepeatMasker output files. *Mobile DNA* 5:13.
- 1172 100. Palmer JM, JE S. 2016. Funannotate: Eukaryotic genome annotation pipeline.  
1173 <http://funannotate.readthedocs.io>. Accessed
- 1174 101. Cook DE, Valle-Inclan JE, Pajoro A, Rovenich H, Thomma B, Faino L. 2019. Long-  
1175 Read Annotation: Automated Eukaryotic Genome Annotation Based on Long-Read cDNA  
1176 Sequencing. *Plant Physiol* 179:38-54.
- 1177 102. Haas BJ, Salzberg SL, Zhu W, Pertea M, Allen JE, Orvis J, White O, Buell CR, Wortman  
1178 JR. 2008. Automated eukaryotic gene structure annotation using EVIDENCEModeler and the  
1179 Program to Assemble Spliced Alignments. *Genome Biology* 9:R7.
- 1180 103. Shannon P, Markiel A, Ozier O, Baliga NS, Wang JT, Ramage D, Amin N, Schwikowski  
1181 B, Ideker T. 2003. Cytoscape: A software environment for integrated models of biomolecular  
1182 interaction networks. *Genome Research* 13:2498-504.
- 1183 104. Team RC. 2013. A Language and Environment for Statistical Computing }.
- 1184 105. Wickham H. 2016. ggplot2: Elegant Graphics for Data Analysis }.
- 1185 106. Gel B, Serra E. 2017. karyoploteR: an R/Bioconductor package to plot customizable  
1186 genomes displaying arbitrary data. *Bioinformatics* 33:3088-3090.
- 1187 107. Hahne F, Ivanek R. 2016. Visualizing genomic data using Gviz and Bioconductor.  
1188 *Methods in molecular biology (Clifton, NJ)* 1418:335-351.
- 1189 108. Sullivan MJ, Petty NK, Beatson SA. 2011. Easyfig: A genome comparison visualizer.  
1190 *Bioinformatics* 27:1009-10.
- 1191 109. Kurtz S, Phillippy A, Delcher AL, Smoot M, Shumway M, Antonescu C, Salzberg SL.  
1192 2004. Versatile and open software for comparing large genomes. *Genome Biology* 5:R12.
- 1193 110. Drillon G, Carbone A, Fischer G. 2014. SynChro: A fast and easy tool to reconstruct and  
1194 visualize synteny blocks along eukaryotic chromosomes. *PLoS One* 9:e92621.

1195 111. Drillon G, Champeimont R, Oteri F, Fischer G, Carbone A. 2020. Phylogenetic  
1196 reconstruction based on synteny block and gene adjacencies. *Molecular Biology and Evolution*  
1197 doi:10.1093/molbev/msaa114.  
1198

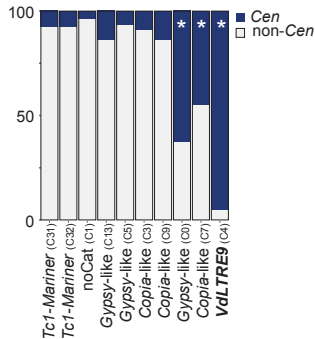


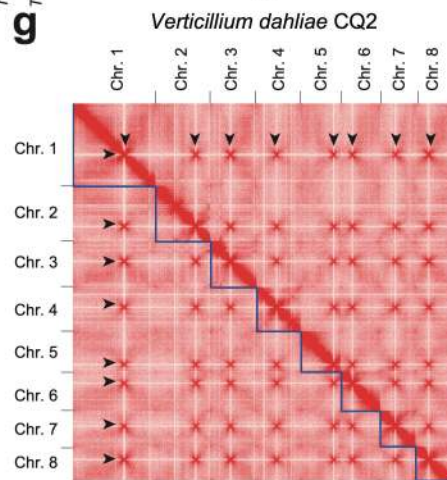
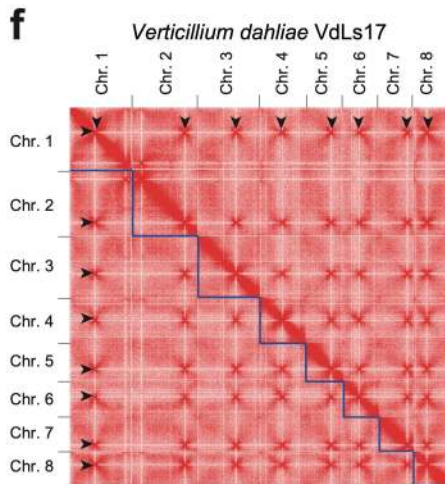
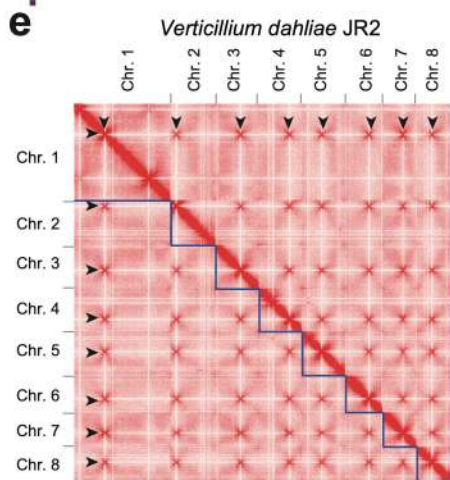
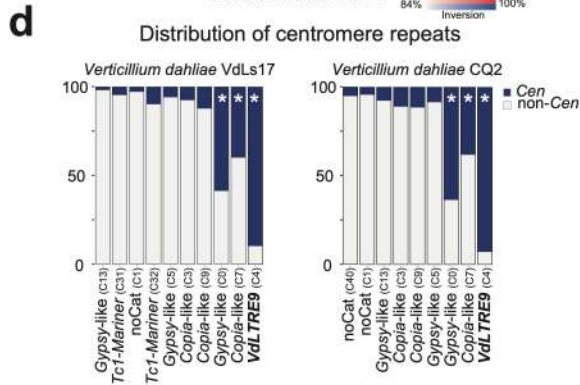
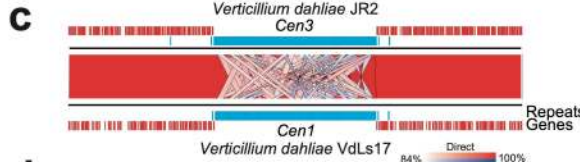
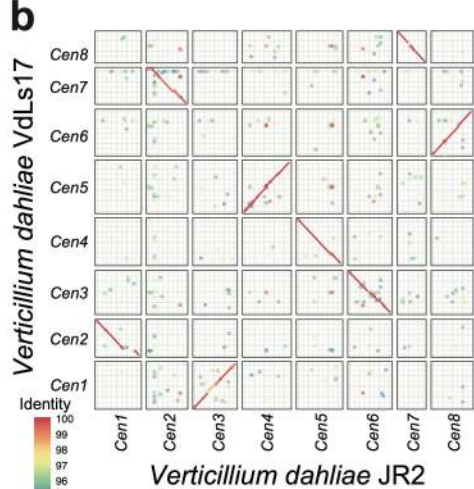
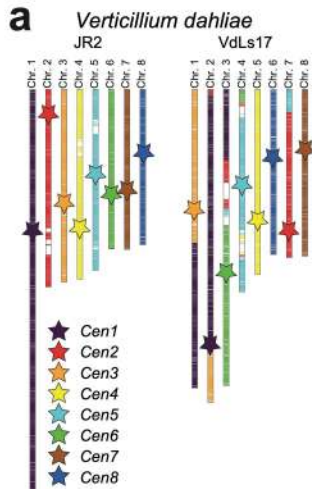


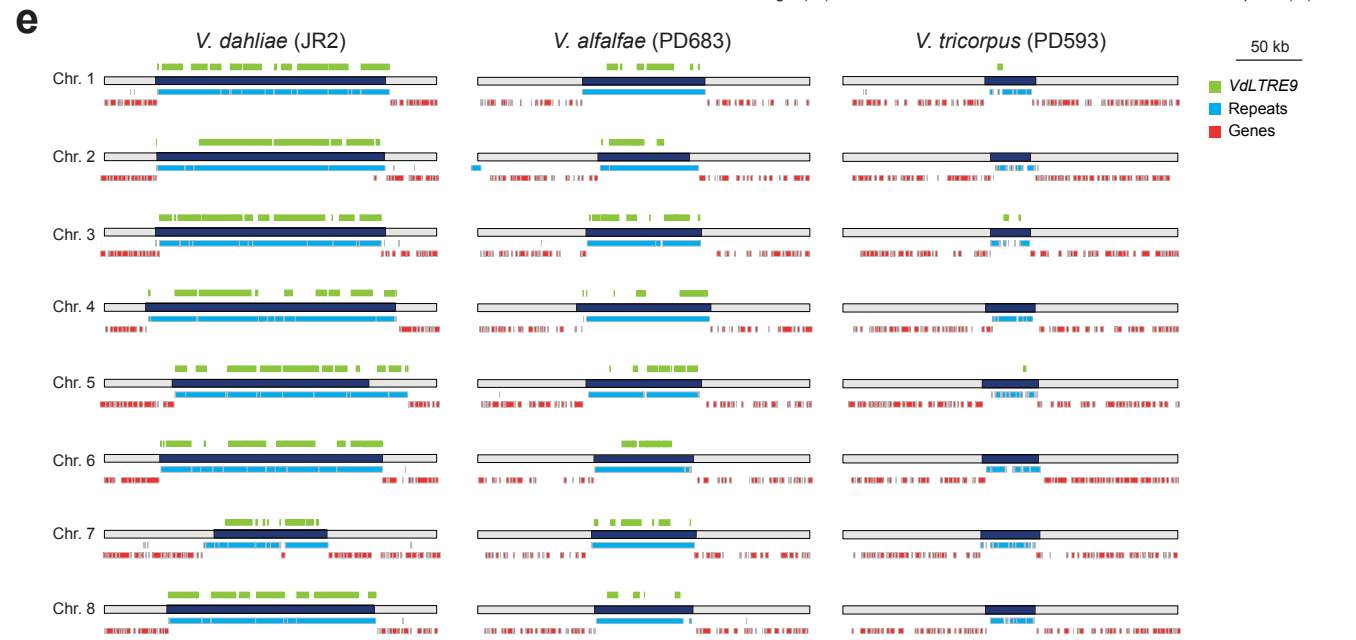
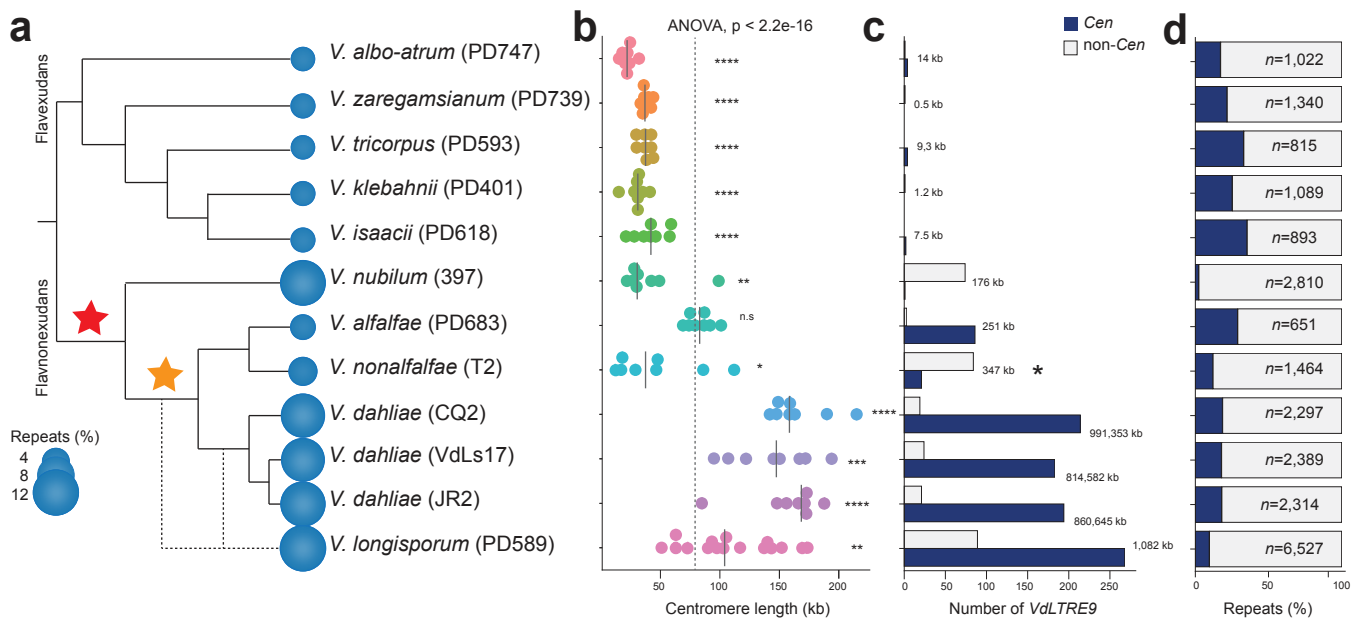


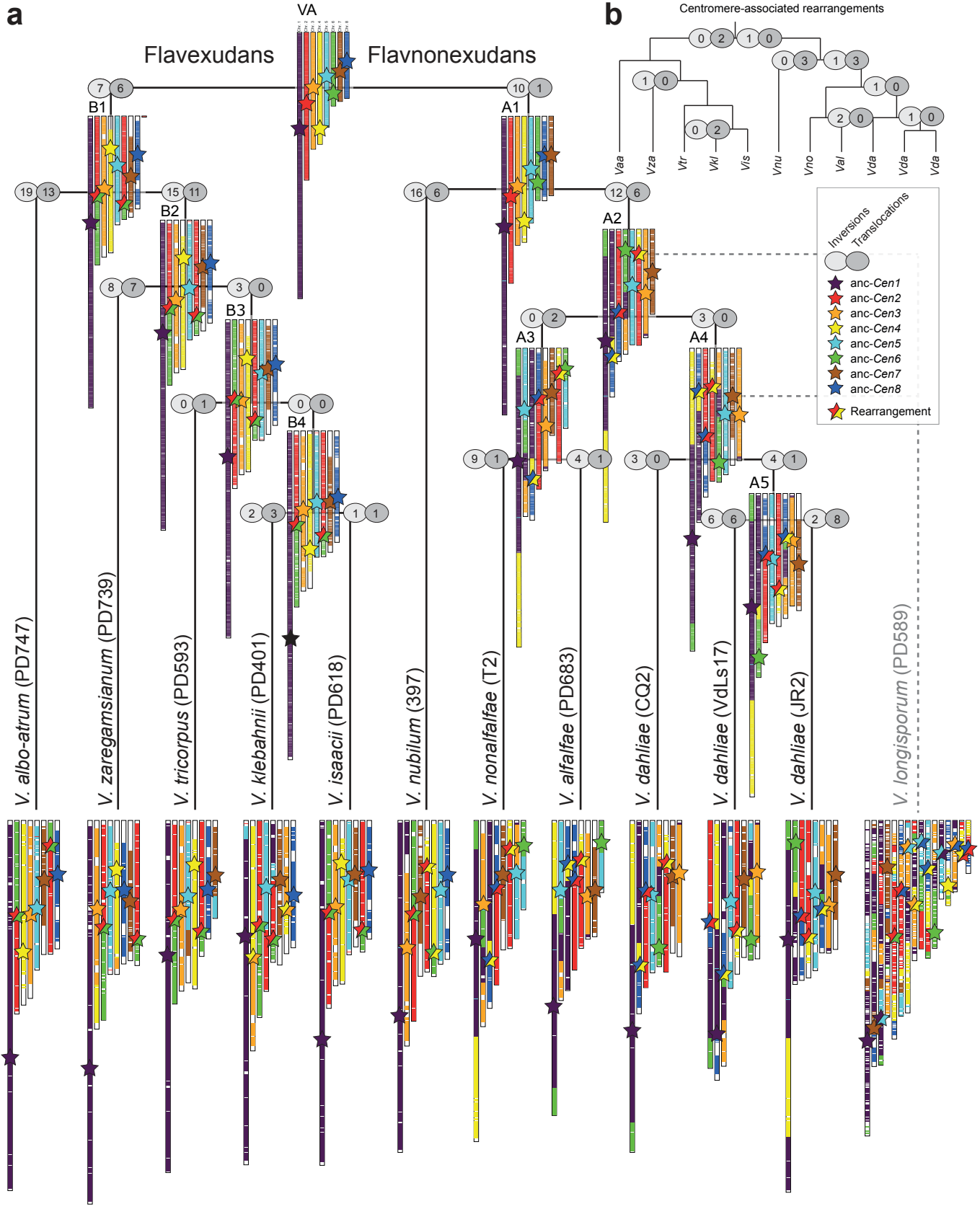
**a****b****c**

Distribution of centromere repeats







**a**

**Table 1: Genome characteristics of the centromeres of *Verticillium dactylophilum* strain UR2.**

Chr.	Locus	CenH3		AT-rich	AT-content (%) <sup>3</sup>		Repetitive elements	
		CenH3 position (bp) <sup>1</sup>	CenH3 length (bp)	Position (kb) <sup>2</sup>	Chr.	Cen.	# Repeats (%) <sup>4</sup>	# VdLTRE9 (%) <sup>4</sup>
1	<i>CEN1</i>	2,920,143-3,094,179	174,037	2,919-3,094	45.7	77.1	50 (99.8)	27 (70.4)
2	<i>CEN2</i>	520,698-672,281	151,584	516-672	46.3	77.8	43 (99.7)	26 (83.0)
3	<i>CEN3</i>	2,374,294-2,541,026	166,733	2,375-2,542	45.8	77.3	47 (99.8)	31 (80.5)
4	<i>CEN4</i>	2,884,316-3,071,412	187,097	2,885-3,072	46.2	75.4	54 (99.5)	24 (53.8)
5	<i>CEN5</i>	1,868,317-2,043,260	174,944	1,868-2,044	46.7	73.9	58 (99.5)	25 (63.1)
6	<i>CEN6</i>	2,166,972-2,333,060	166,089	2,167-2,334	46.4	75.2	48 (100)	31 (62.6)
7	<i>CEN7</i>	1,944,367-2,038,091	93,725	1,945-2,038	44.7	76.5	32 (95.8)	14 (47.8)
8	<i>CEN8</i>	1,406,398-1,561,664	155,267	1,406-1,562	47.7	77.0	37 (100)	26 (73.9)

<sup>1</sup>: position of CenH3-enriched domains; enriched domains within 10 kb have been merged

<sup>2</sup>: position of AT-rich domains; AT-rich domains with 20 kb have been merged

<sup>3</sup>: average AT-content of 1 kb windows of the entire chromosome and the AT-rich domain

<sup>4</sup>: percentage of centromeric region covered